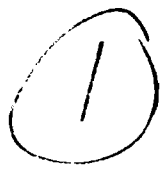DTIC
ELECTE
JAN 0 6 1992
S
D
D

SELF-PUMPED PHASE-CONJUGATE
TWYMAN-GREEN INTERFEROMETRY
USING A BaTiO$_3$ CRYSTAL

THESIS

Deborah A. Determan, Captain, USAF

AFIT/GEP/ENP/91D-3

Approved for public release; distribution unlimited

SELF-PUMPED PHASE-CONJUGATE
TWYMAN-GREEN INTERFEROMETRY
USING A BaTiO$_3$ CRYSTAL

THESIS

Presented to the Faculty of the School of Engineering

of the Air Force Institute of Technology

Air University

in Partial Fulfillment of the

Requirements for the Degree of

Master of Science in Engineering Physics

Deborah A. Determan, B.S.

Captain, USAF

December 1991

Preface

The purpose of this study was to demonstrate a phase-conjugate Tywman-Green interferometer using a $BaTiO_3$ crystal and to use this interferometer to test various optical components. This was done using both collimated and divergent beams as the primary beam. This method of testing optical quality will provide the Air Force with a versatile tool that eliminates the need for high quality optics when using conventional Twyman-Green interferometry to test concave mirrors. Testing was performed to determine optical quality of various convergent lenses, plane parallel plates, and planar and concave mirrors.

In performing this experimentation and writing this thesis, I have had a great deal of help from others. I am deeply indebted to my faculty advisor, Dr. Won Roh, for his patience and assistance throughout this learning process. A word of thanks to the laboratory technicians, especially Mr. Greg Smith, for their patience and cheery helpfulness. I feel a special thanks is due to all my classmates. Their support, helpful ideas, and comraderie have made this program an enjoyable experience, as well as a learning one.

Most importantly, I wish to thank my husband, Jon. His ceaseless support, understanding, and efforts to make this program easier for me are deeply appreciated.

<div align="right">Deborah A. Determan</div>

Table of Contents

List of Figures

List of Tables

Abstract

This study demonstrated a phase-conjugate Tywman-Green interferometer using a $BaTiO_3$ crystal in the reference arm and this interferometer was used to test various optical components. This was done using both collimated and divergent beams as the primary beam. Testing was performed to determine optical quality of various convergent lenses, plane parallel plates, and planar and concave mirrors. Divergent beam phase-conjugate interferometry provided a schematic to test concave mirrors without the need of additional high quality optics normally needed for this type of testing using conventional Twyman-Green interferometers. Additionally, a phase-conjugate interferometer is able to detect with twice the sensitivity any defect in the primary beam. This property makes the phase-conjugate interferometer is a highly sensitive test for collimation.

SELF-PUMPED PHASE-CONJUGATE TWYMAN-GREEN INTERFEROMETRY USING A BaTiO$_3$ CRYSTAL

I. Introduction

The Air Force uses optical imaging systems in many fields such as communications, target recognition, and missile guidance. For proper execution of these applications, the optical imaging systems used in these fields must be of extremely high quality so that an ideal image is obtained.

An ideal optical imaging system is one that transforms each point of a wave leaving the object plane into a corresponding point in the image plane. A deviation from the ideal image is known as an aberration, which can result from many factors such as bad system design or irregular optical surfaces.

Determining the quality of optical components by the use of interferometry was pioneered by Twyman in 1918, and the Twyman-Green interferometer is still widely used as a powerful tool to determine the amount of aberration found in optical components. A major drawback with this tool is that the optical components which comprise the interferometer must not introduce aberration into the interfering beams.

A phase-conjugate Twyman-Green interferometer can use collimated or divergent beams to test optics due to the

1

property that the phase-conjugate mirror returns a time-reversed replica of the original beam. In divergent beam configurations, this type of interferometer would eliminate the need for the high quality reference optics needed in conventional Twyman-Green interferometry. A phase-conjugate Twyman-Green interferometer would provide the Air Force with a simple and versatile tool useful for determining the quality of the optics used in its various applications of optical imaging systems.

The objective of this thesis is to demonstrate phase-conjugate Twyman-Green interferometry using a barium titanate ($BaTiO_3$) crystal as the phase-conjugating mirror in the reference arm of the interferometer and to use this interferometer to test the optical quality for a number of diverse optical components.

This thesis begins in Chapter II with a review of interferometry and aberrations, a discussion of self-pumped phase-conjugation and its application to interferometry, as well as a review of the relevant work performed in this area. The experimental apparatus is detailed in Chapter III, while Chapter IV describes the experimental procedure used in this study. Chapter V contains the experimental results and the discussion. The final chapter presents observations, and conclusions.

II. Theory

A review of interferometry and aberrations is presented in this section, followed by a discussion of self-pumped phase-conjugation and its application to Twyman-Green interferometry. The final section presents a background review of the previous work in optical phase-conjugate interferometry.

2.1 Optical Interferometry

Interference and coherence are "the experimental and theoretical aspects of the same phenomenon" (Steel 1983:3). Two beams are considered coherent for the time period that the difference between their phase angles remains constant, and the average of this time period is called the coherence time. Coherent beams interfere with each other such that the combined beam has regions of minimum and maximum intensity that differ from the sum of the individual beam intensities. Optical interferometers are tools used to study this interference of light.

An amplitude splitting interferometer, such as a Twyman-Green, divides a primary beam into two sections which travel different paths before reuniting and interfering as in Figure 1. Light from the same source that travels different paths may be coherent if the source has a sufficiently long coherence time. The reunited beam has a total relative irradiance, I, given by (within the

Plane Mirror

Beam Splitter

Primary Beam

Plane Mirror

Observation Screen
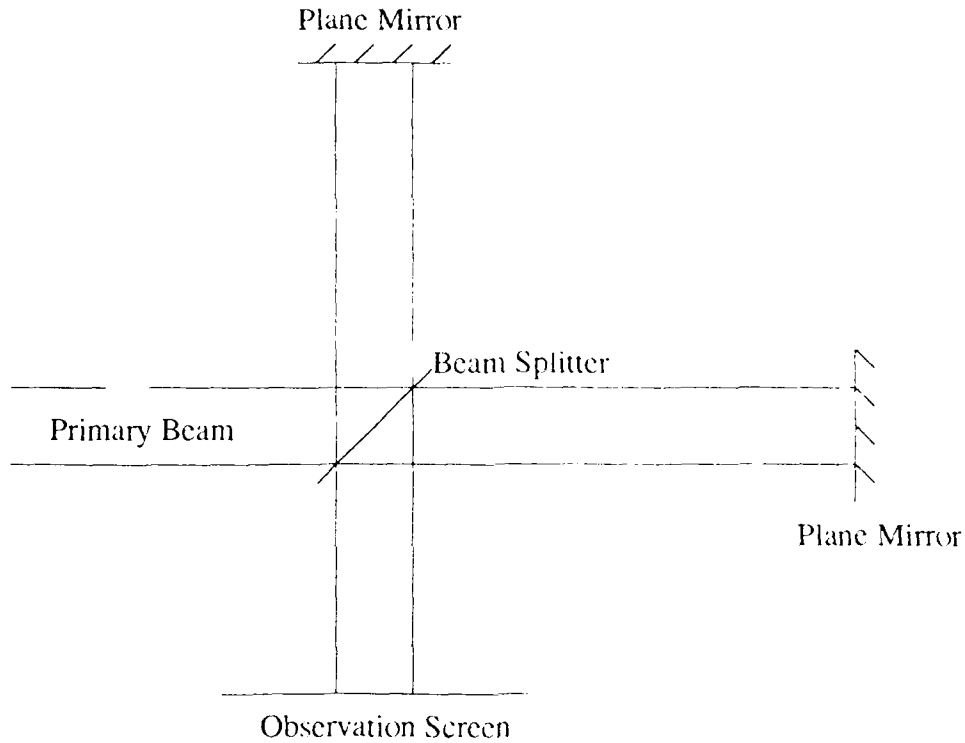
Figure 1.   An Amplitude Splitting Interferometer

same medium) the time average of **E · E**, and for two coherent

beams in this type of interferometer is given by

$$I = E_1^2 + E_2^2 + 2\boldsymbol{E_1} \cdot \boldsymbol{E_2} \cos (\boldsymbol{k_1} \cdot \boldsymbol{r} - \boldsymbol{k_2} \cdot \boldsymbol{r} + \epsilon_1 - \epsilon_2) \qquad (1)$$

where the subscripts represent beam 1 and 2 respectively,

E is the vector sum of the individual electric field

intensities and has magnitude E, k represents the

propagation vector, r is the position vector, and ϵ

represents the initial phase angle.   The term with the

cosine is called the interference term and the argument of

4

the cosine in the interference term is called the phase difference, d, between the two beams at point r.

For incoherent beams, the time average of the cosine term is zero and the total relative irradiance reduces to the sum of the irradiances of the constituent beams, but for coherent beams, equation 1 reduces to

$$I = I_1 + I_2 + 2(I_1 I_2)^{1/2} \cos(d) \qquad (2)$$

The maximum irradiance occurs when d = $2m\pi$, where m = 0,1,2... (total constructive interference), and the minimum irradiance occurs when d = $(2m + 1)\pi$ (total destructive interference).

The regions of maximum and minimum irradiance produce fringe patterns from which physical quantities such as the phase variations can be derived (Steel 1983:2). The variations in phase provide information on the aberrations present in the optic system and are used to determine optical quality.

2.2 Aberrations

The primary third-order aberrations are known as Seidel aberrations and include spherical aberration (SA), coma, astigmatism, field curvature, and distortion. The first three of these are image degrading aberrations due to spherical optics (lenses and mirrors).

Spherical aberration is caused by nonparaxial rays (in the absence of any other aberration) focusing in line with, but to different distances from, the paraxial focus. Minimized spherical aberration occurs for spherical lenses that produce an emerging ray that makes close to the same angle to the exit face normal as does the incident ray to the entrance face normal.

Spherical aberration is present in convergent lenses because the marginal rays are bent too much (positive SA), focusing in front of the paraxial rays. A divergent lens has negative SA due to the marginal rays intersecting the axis behind the paraxial focus (Hecht 1979:176). Figure 2 shows positive SA for a planar-convex lens.
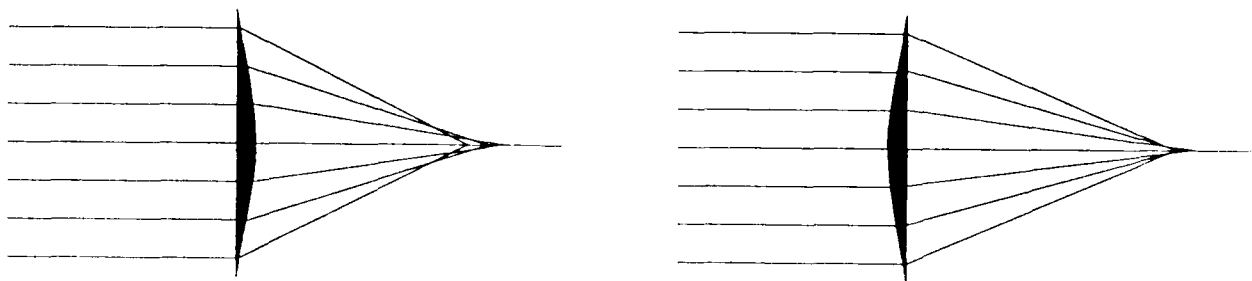
Figure 2. Positive SA for a planar-convex lens

Whereas spherical aberration is evident when marginal rays focus at different distances in line with the paraxial focus, coma is evident when marginal rays focus at the paraxial focal length, but at different distances from the

optic axis than that of the paraxial focus. Each bundle of
rays that focus to a different point have a different
transverse magnification. Figure 3 depicts positive
(marginal rays focus further from the axis) and negative
(focus of marginal rays at a distance closer to the optic
axis) coma.

(a)   (b)
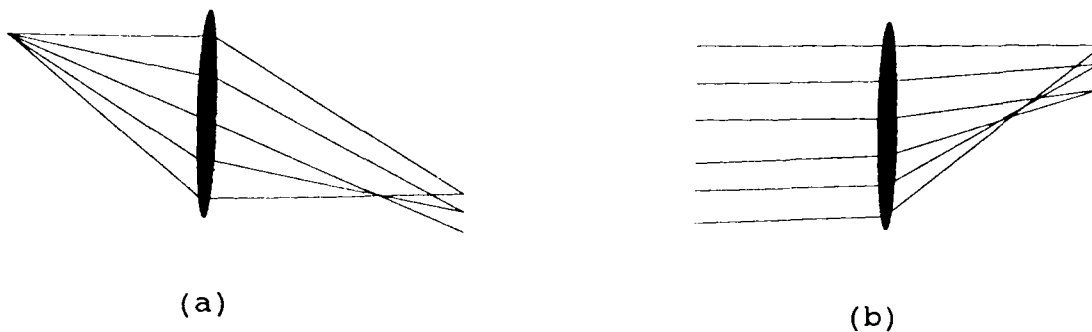
Figure 3. Positive (a) and Negative (b) Coma

Astigmatism gives rise to two distinct focal lengths
for a cone of rays; the radius of curvature in the
tangential plane is different for that in the sagittal
plane. As the beam is focusing, the cross-section becomes
elliptical with the major axis in the sagittal plane until
it coalesces into a horizontal line, which is identified as
the tangential focus (Hecht 1979:181). As the rays leave
this point, they become circular then again coalesce into a
line, which is vertical and known as the sagittal focus.

7

The point where the rays are circular and make the minimum blur is known as the best focus, or circle of least confusion. Figure 4 depicts astigmatism.
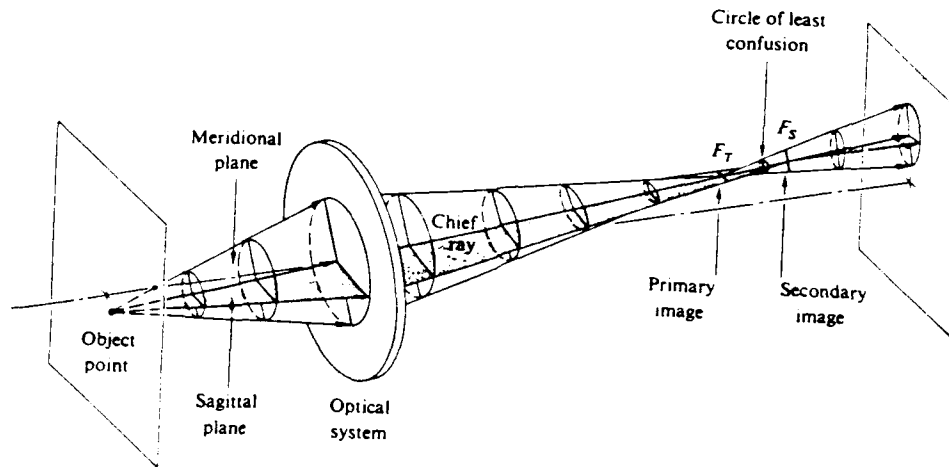
Figure 4.   Astigmatism (Hecht 1979:182)

Besides the three Seidel image degrading aberrations, two other aberrations, tilt and defocus, are commonly found in amplitude splitting interferometers. Tilt between two wavefronts may be expressed as an angle or as a distance. Tilt produces equidistant infinite parallel fringes when no other aberration is present. Defocus involves interference between two waves where one has a slightly different spherical wavefront. Figure 5 shows typical Twyman-Green type interferograms for spherical aberration, coma, astigmatism, tilt, and defocus.

8
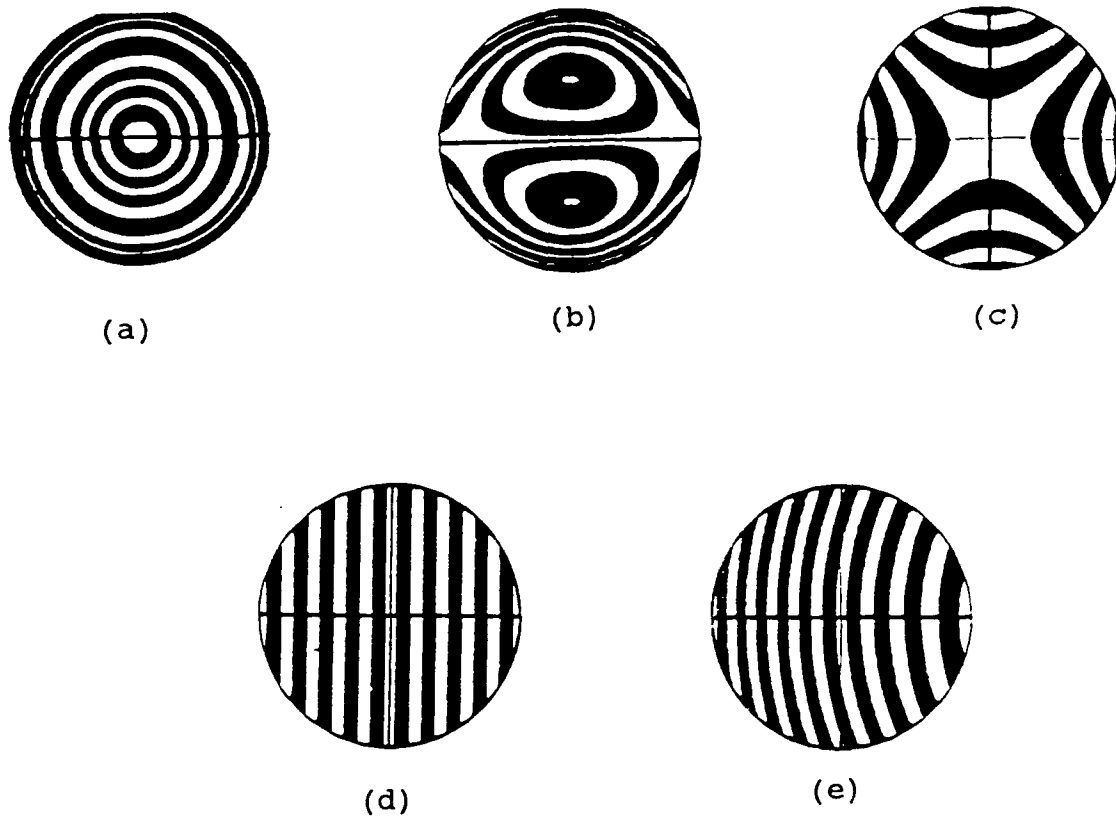
Figure 5. Typical Twyman-Green interferograms depicting
Spherical Aberration (a), Coma (b), Astigmatism (c),
Tilt (d), and Defocus (e) (Wyant 1987:76,85)

2.3   Phase-conjugation

Optical phase-conjugation is a process where the
reflected beam is an exact replica of the incident beam
traveling in the opposite direction and is depicted in
Figure 6.

9

ordinary
mirror

phase-
conjugate
mirror
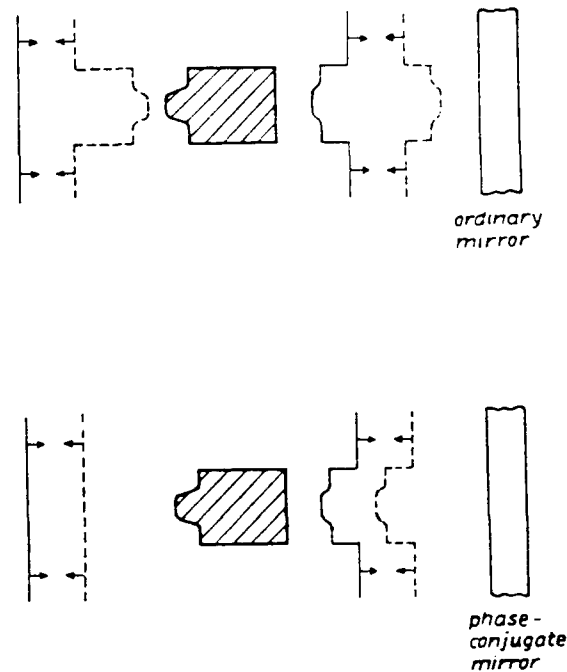
Figure 6. Phase-conjugate and ordinary mirror reflections
(Schubert 1986)

The wavefront of the reflected beam maps in space
exactly to that of the incident beam. A phase-conjugate
beam can be thought of as a time-reversed replica of itself,
eliminating aberrations and misalignments the original beam
encounters prior to phase-conjugation. This process can be
implemented using four-wave mixing in photorefractive
materials, such as $BaTiO_3$.

Photorefractive materials are those whose refractive
index changes in response to intensity of light, and this
change is usually semipermanent (Pepper 1990:62). Light in
the material generates free charges which subsequently move
from bright to dark regions through diffusion and gradually
build up an electric field that can change the index of

refraction through the electro-optic effect. A sinusoidal intensity grating in the crystal can give rise to an index grating which is phase shifted 90 degrees from the intensity grating. Photorefractive crystals such as $BaTiO_3$ can generate the phase-conjugate of an incident signal beam without requiring the usual "pump beam" in a so called self-pumped four-wave mixing geometry (Feinberg 1983: 480).

Using a phase-conjugate mirror in a Twyman-Green interferometer has many implications. The quality of any optic placed in the reference arm containing the phase-conjugate mirror is unimportant. In the ideal case, any aberrations introduced prior to the crystal correct themselves upon phase-conjugation. The crystal always returns a beam that exactly matches that which entered the reference arm, eliminating alignment considerations.

Another implication of phase-conjugate interferometry is that divergent light can be used as the input beam to both arms. In conventional Twyman-Green interferometry, a collimated beam enters and exits both arms of the interferometer. When a spherical surface is tested, the collimated beam in the test arm is made to diverge in order to test the surface shape of the test object and then return collimated by using other optics in an afocal configuration with the mirror. Using divergent phase-conjugate interferometry eliminates the need for these other optics, which need to be of extremely high quality. In this type of interferometry, the crystal returns a convergent beam that

focuses to the point of the original beam's divergence. If the test object is located so that its return beam focuses at the same point as the phase-conjugate crystal, testing can be accomplished without using additional optics.

2.3   Previous Work in Phase-conjugate Interferometry

Phase-conjugate interferometry was first discussed theoretically in scientific literature in the early 1980's. In 1980, Hopf described two theoretical examples of a Mach-Zehnder phase-conjugate interferometer, using degenerate three- and four-wave mixing, noting that these phase-conjugate interferometers would be self-referencing, sensitive to small changes in the phase front, yet fringe contrast would be unaffected by variations in the signal intensity. The following year this concept was demonstrated successfully (Bar-Joseph et al 1981). Feinberg demonstrated a self-pumped phase-conjugate Michelson interferometer in 1983 which eliminates the air turbulence effects or the need for high quality optics in the reference arm.

In 1986, Howes discussed theoretically a phase-conjugate Twyman-Green interferometer that would be a sensitive method of determining lens collimation. A phase-conjugate Fizeau interferometer was demonstrated in 1989 to characterize the wavefront of an aberrated optical system (Gauthier et al 1989).

The phase-conjugate interferometers used in the above demonstrations and applications were accomplished using a

collimated input beam. Phase-conjugate Twyman-Green interferometers using divergent light to test spherical surfaces was first demonstrated in 1990 (Shukla et al). These interferometers eliminate the necessity of large reference spherical mirrors when testing these surfaces as well as the need for a compensating plate normally required when passing divergent light through a beam splitter in this type of interferometer.

III.   Experimental Apparatus

A schematic of the basic experimental set-up is presented in Figure 7. An Ion Laser Technology Model 5490AWC argon ion laser, with 60mW power operating multimode at 514.5 nm, was used in this experiment. A Spectra Physics Model 310-21 Polarization rotator was used to horizontally polarize the laser beam in order to produce an extraordinary ray incident on the crystal, which was aligned such that its +C axis was in the horizontal plane.
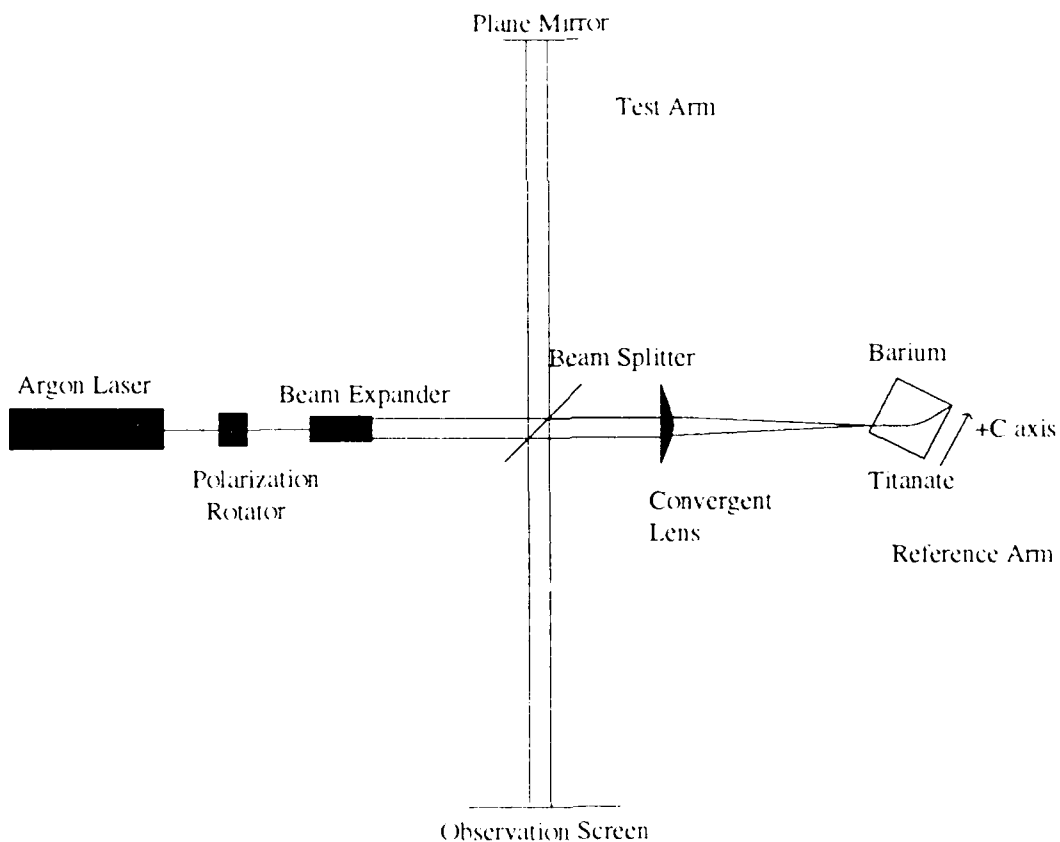

Figure 7.   Basic Experimental Set-Up

14

A Jodon beam expander employing a 20X microscope objective and a 25 micron pinhole was used to expand the laser beam. A beam splitter with a high transmittance (85% at 45 degrees) was used to send most of the beam power to the $BaTiO_3$ crystal, which has a much lower reflectivity than the mirrored surfaces used in the test arm of the interferometer. Reflectivities for phase-conjugated beams in $BaTiO_3$ have been reported in the range of 50-70% (Wink 1988:24), while laboratory quality mirrors have reflectivities on the order of 99%. A variable neutral density filter was used in the test arm of the interferometer to reduce, and match, the intensity reflected from the test arm to that of the returned reference beam.

A convergent lens was used to focus the reference beam onto the $BaTiO_3$ crystal at an angle of about 55 degrees with respect to +C axis of the crystal. The $BaTiO_3$ crystal used was manufactured by Sanders Associates, ID# 162-D, was z-cut and measured 7.0 mm x 7.0 mm x 5.5 mm.

A Micro-Control stepper-motor, Klinger model UE72, controlled by a Programmable Stepping Motor Controller (model MC4) and Power Driver (model MD4), was used for fine adjustments (step size of .1 micron) of optical components along the test arm axis. The optical components used as test objects in this thesis are detailed in Appendix A.

A General Electric Charge Injection Device (CID) camera, model TN2509, was used as the input device for a frame grabber (BeamCode 5.0 developed by Big Sky

Corporation). The frame grabber was used to record the interference pattern of the interferometer at the observation plane.

A SummaGraphics MM 1201 Graphics tablet was used to digitize the recorded fringe patterns. These digitized fringe patterns were analyzed for their Seidel coefficients using the WYCO Interferogram Software Package, WISP-PC version 2.31. This program used an expansion of the first eight Zernike polynomials to determine the Seidel coefficients. The analysis method used by this software is detailed in Appendix B.

IV.   Experimental Procedure

4.1   Basic Experimental Set-Up

Self-pumped phase-conjugation was demonstrated to establish the crystal's ability to produce the phase-conjugate reflection required for interference. This was accomplished for direct laser (Gaussian) and image bearing beams. The beam returned from the crystal is referred to as the reference beam of the interferometer. With phase conjugation established, a plane mirror was incorporated into the experiment as the test arm of the interferometer, as shown in Figure 7.

4.2   Collimation

For a Twyman-Green interferometer which uses a phase conjugating mirror in the reference arm, the beam reaching the observation point from the plane mirror is divergent (convergent) and the phase-conjugated beam is convergent (divergent) when the input beam is not collimated, but is divergent (convergent) (Howes 1986:474). When the beam is perfectly aligned and collimated, the beams from both arms of the interferometer are collimated and by introducing tilt, parallel infinite fringes are observed.

In the basic experimental set-up, a collimated beam resulted if the distance between the collimating lens of the Jodon beam expander and the pinhole was exactly equal to the focal length of the collimating lens. Initially,

collimation was determined by measuring the diameter of the expanded beam (1 cm at origin) with a centimeter ruler at several distances (final distance of 10 meters) from the source, adjusting the distance between the collimating lens and the pinhole to attain diameter measurements that were the same. Using this beam as the input to the basic set-up, and introducing a tilt to the test arm mirror, finer adjustments on the distance between the collimating lens and pinhole were performed until parallel infinite fringes were evident.

4.5   Plane Parallel Plates

When a plane parallel plate is introduced into the test arm of the interferometer shown in Figure 7, the optical path difference (OPD) introduced by the plate to the test beam is given by

$$OPD = 2(n-1)t \qquad \textbf{(3)}$$

where t is the plate thickness and n is the refractive index of the plate. When a collimated beam is used with the interferometer adjusted so that no fringes are observed before the plate is inserted into the test beam, any fringes that are observed after it is inserted are due to the plate. If no fringes are observed, it indicates that the OPD is constant over the area that the beam passes through on the plate. Any fringes that do appear give information about the plate. If the fringes are distorted, it is an indication that the plate has nonuniform thickness or is inhomogeneous

(its refractive index is not constant throughout the area the beam passes through). If the fringes are straight, it indicates that the plate has flat surfaces but that they are separated by an angle θ such that

$$\theta = \frac{\lambda}{2(n-1)\Delta s} \qquad (4)$$

where λ is the wavelength of the beam, and Δs is the fringe spacing.

Several plane parallel plates were tested during this thesis research. These included a plane parallel plate of glass, a microscope slide overlaid with a piece of cellophane tape, and a thin film of soap.

4.4 Convergent Lenses

A convergent lens was placed in the test arm of the basic experimental set-up, parallel to the planar mirror and at a distance from the planar mirror equal to its focal length, as shown in Figure 8.

The return beam was collimated after passing through the lens only if the mirror and lens were configured as above. This configuration for testing convergent lenses reveals symmetric aberrations such as astigmatism and third order spherical (Malacara 1978:61). For a good quality lens, these aberrations are absent and infinite parallel fringes result when tilt is introduced.
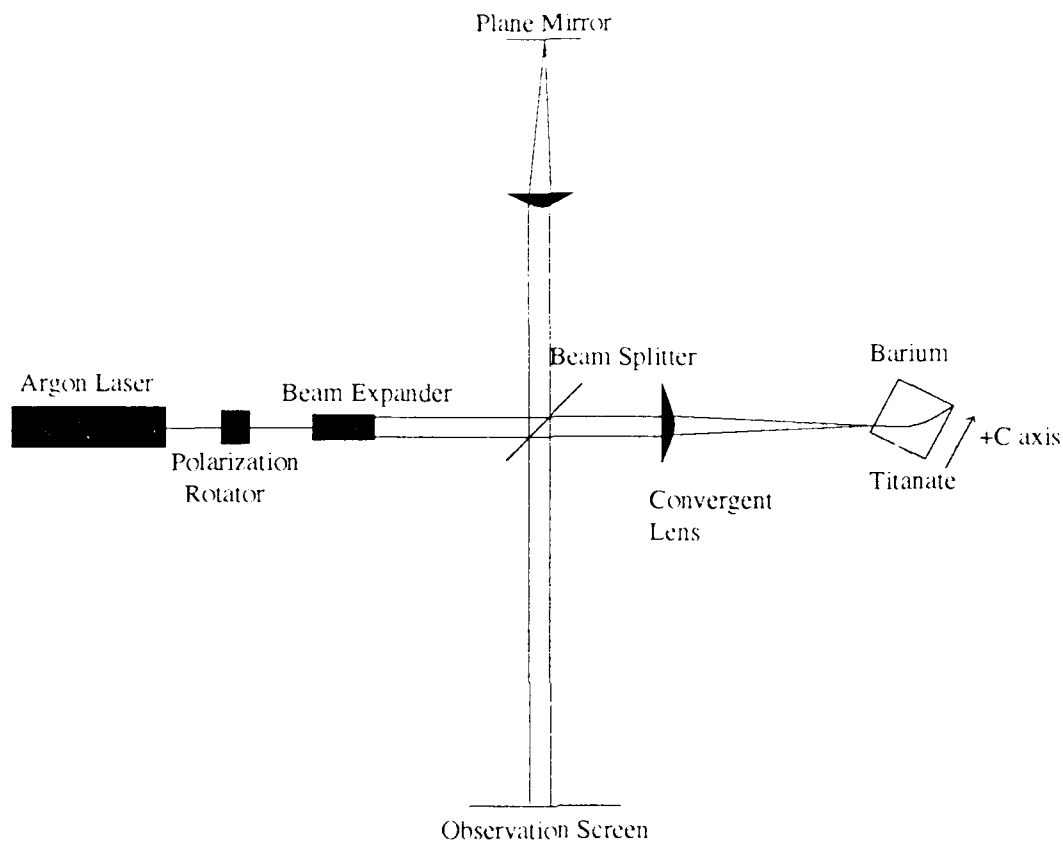
Figure 8.   Interferometry configuration for testing convergent lenses

Convergent lenses of various quality and focal length were tested. Plano-convex lenses were tested twice, once each with the planar or the convex side facing the incident beam.

20

4.5   Mirrors

Two mirror shapes, planar and concave spherical, were tested for surface quality. For testing a plane mirror, the system shown in Figure 7 was used with the flat mirror replaced with the test piece. Two planar mirrors were tested, the laboratory quality mirror used for collimation testing and a commercial drug store quality mirror.

The interferometry configuration for testing the concave spherical mirror involved replacing the planar mirror of the basic experimental set-up with a concave spherical mirror and introducing a divergent beam into the two arms of the interferometer, as shown in Figure 9.

The divergent beam used in testing the concave spherical mirror was produced by removing the collimating lens of the beam expander and focusing the laser beam through the microscope objective onto a pinhole, which provided a spatially filtered divergent beam. The return beam from the test mirror had two points of focus. By adjusting the optical path length between the concave mirror and the pinhole so that it was equal to the radius of curvature of the concave mirror, the return beam focused back onto the pinhole when reflected at the beam splitter, and the transmitted return beam focused at a distance from the beam splitter equal to the distance between the point of reflection at the beam splitter and the pinhole.

In the reference arm, the initial diverging beam transmitted through the beam splitter focused onto the
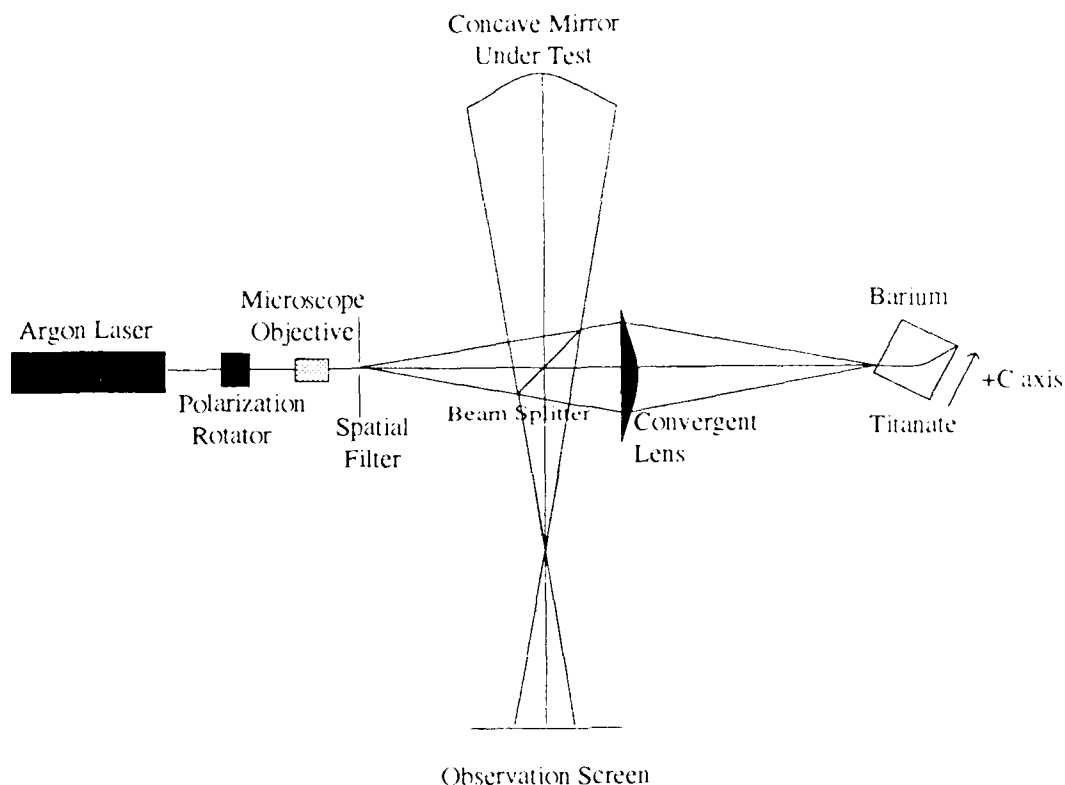
21

Figure 9.   Phase-conjugate divergent beam interferometer
schematic for testing concave mirrors

BaTiO$_3$ crystal by a convergent lens, which did not need to

be of high quality. The reflected phase-conjugate beam was

aberration-free, converging, and focused to the same points

that the test beam focused to when the mirror was placed as

in Figure 9.   The property that phase-conjugate beams time-

reverse themselves ensured that the reference arm beam

focused to the pinhole (and the point equidistant by beam

splitter reflection) no matter what the optical path length

(OPL) between the pinhole and crystal.   The OPL of the

reference arm was kept roughly the same as the test arm for best fringe contrast and coherence length requirements.

The beam splitter, which has a reflective coating on one side, was positioned so that the test beam was reflected from the front face. This type of beam splitter in an interferometer produces one beam that travels through the beam splitter once, and another that travels it three times. In a conventional Twyman-Green interferometer, a compensator plate identical to the beam splitter substrate needs to be placed in the arm that travels through the beam splitter once to correct for the OPD between the two arms. In a phase-conjugate interferometer, the compensator is not necessary with the proper orientation of the beam splitter. This orientation requires that the test arm correspond to the beam that travels the beam splitter once. The property that the phase-conjugate beam is an exact replica of itself as it returns to the beamsplitter results in a reference beam that acts as if it traversed the beam splitter only one time. Reflecting the test beam from the back face of the beam splitter (causing it to travel the beamsplitter three times) introduced an optical path difference between the two beams unrelated to actual aberrations in the test optic.

One concave spherical mirror with a 0.5 m radius of curvature was tested using the configuration in Figure 9.

V.   Results and Discussion

Data for this interferometry testing consists of the output of the frame grabber (Beamcode) and the interferogram analysis routine (WISP). The frame grabber resolved the actual interference pattern into 16 levels of intensity. The printed output from the frame grabber is displayed using 3 levels of intensity to record the fringe contrast more clearly. The maximum intensity is represented by black and the lowest intensity level is white. The cross-hair on the interferogram represents the x- and y- axis of the interferogram, which is also represented to the left of the interferogram by plots of the intensity vs position along each axis. The dotted line in these plots represent a gaussian fit to these intensity profiles. Some of these interferograms show chopped peaks along the x- or y- axis indicating that the CID camera was saturated. Information about the fringe at intensities above this saturated point is unknown.

WISP output includes a three dimensional contour plot of the calculated wavefront as well as plots of the digitized points input to the WISP program. This version of WISP requires that closed or astigmatic fringe shapes be input as a single set of lines forming a wedge pattern. The amount of tilt, defocus, astigmatism, coma, and spherical aberration computed from these digitizations are listed as Seidel coefficients in Tables 1-3. Three independent

24

digitizations of a fringe pattern were performed. A mean
with one standard deviation, using $\sigma_{(n-1)}$ calculations due to
the small sample size, is presented.

Figures are presented showing the recorded
interferogram and intensity vs x- and y- axis plot first,
followed by the contour plot of the wavefront calculated
using the interferogram analysis routine and digitization of
fringes when appropriate.

5.1   Collimation

Figure 10 presents the data for the interference
pattern obtained when the primary beam in the basic
experimental set-up was collimated by measuring beam
diameters.

Figure 11 shows the data obtained when the primary beam
was collimated by the method described above and further
adjustments to the distance between the collimating lens and
the pinhole were performed. Infinite parallel fringes
resulted when the test arm mirror was tilted. The Seidel
coefficients for the data in Figures 10 and 11 are presented
in Table 1.

Even a slight amount of defocus in the input beam
showed in the interference pattern of the combined beams
using a phase-conjugate mirror in the reference arm. The
phase-conjugate mirror doubles the effect of the defocus
since it reflects the slightly defocused beam exactly,
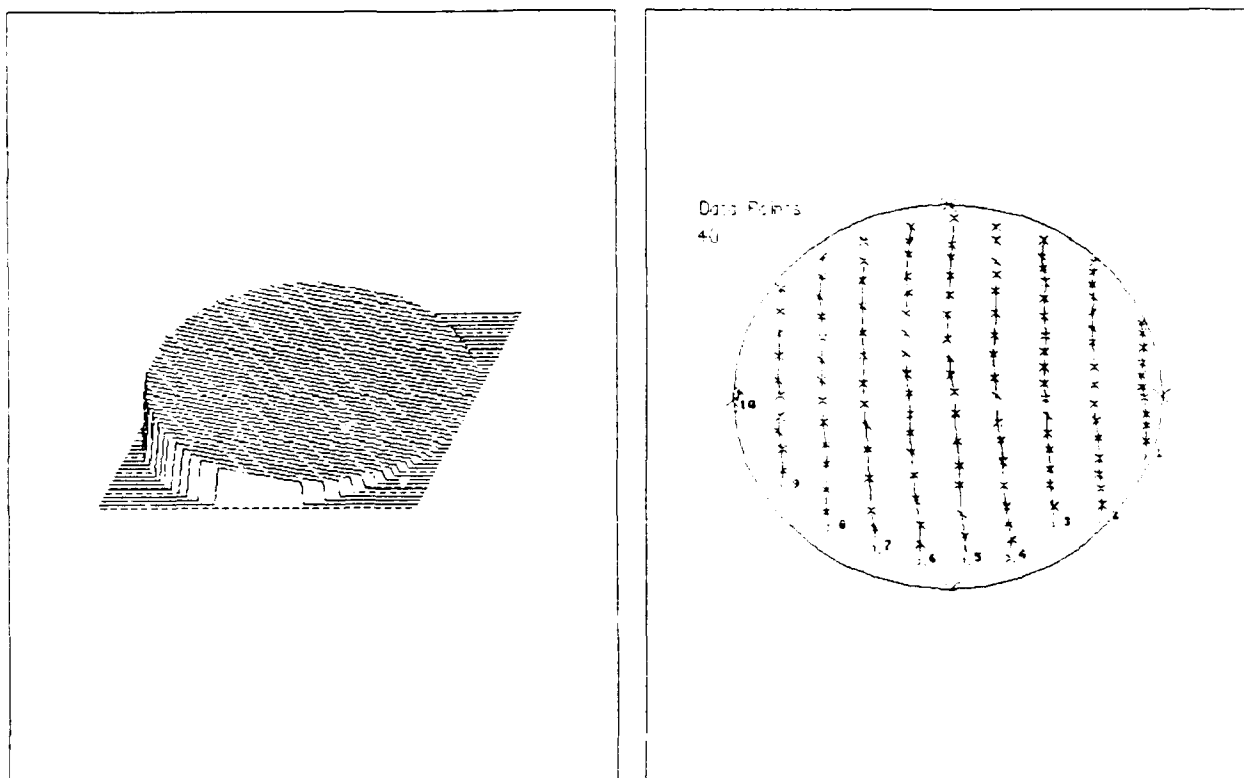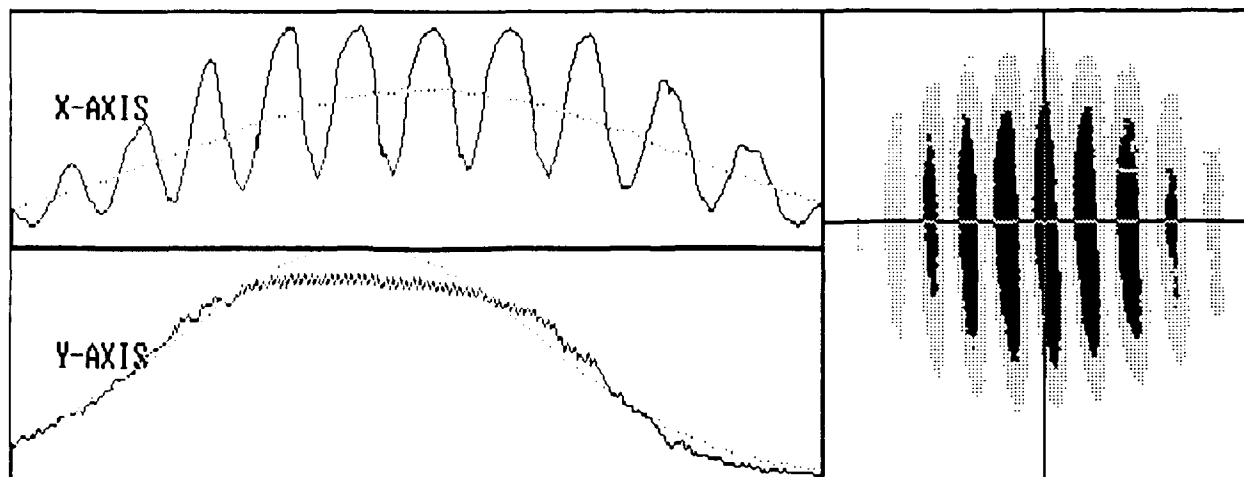causing it to interfere with a mirror reflection of itself.

25

Figure 10. Data for interference using a beam collimated by
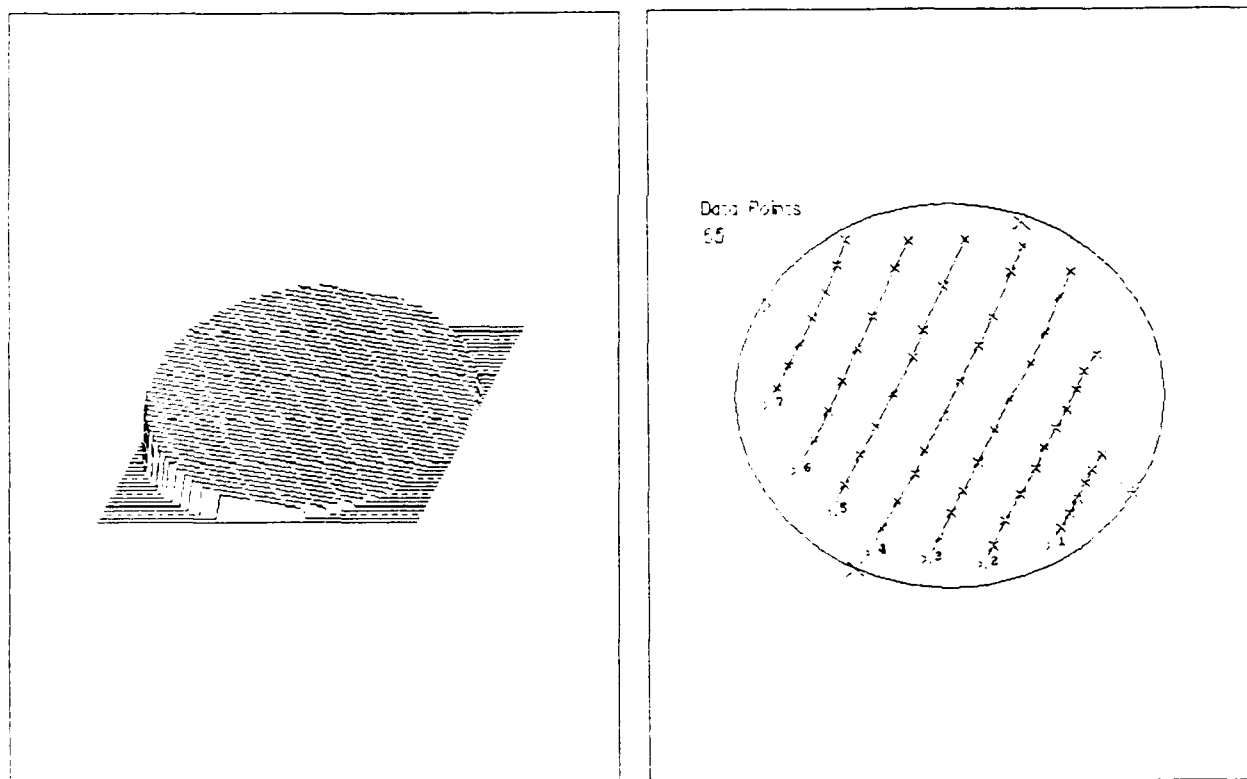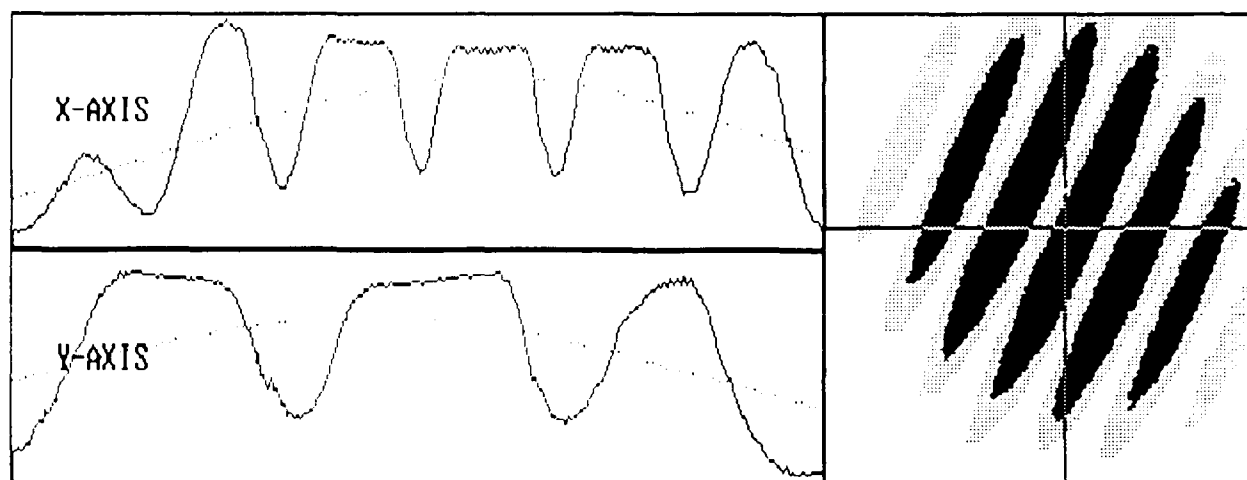beam spot diameter measurement

Figure 11.   Data for interference using a beam collimated by
adjustments to the collimating lenses of a
phase-conjugate interferometer

TABLE 1

SEIDEL COEFFICIENTS (IN WAVES) CALCULATED FROM THE DATA
PRESENTED IN FIGURES 10-12,14

	FIGURE 10 Collimation by diameter measure	FIGURE 11 Collimation by interference	FIGURE 12 Glass plate	FIGURE 14 Thin film
TILT	4.766 + 0.018	3.930 + 0.019	8.168 + 0.038	3.631 + 0.043
DEFOCUS	0.254 + 0.012	0.009 + 0.006	0.043 + 0.017	0.264 + 0.078
ASTIGMATISM	0.087 + 0.004	-0.111 + 0.004	1.009 + 0.052	2.195 + 0.131
COMA	0.116 + 0.026	0.047 + 0.015	0.598 + 0.129	0.990 + 0.055
SPHERICAL ABERRATION	0.047 + 0.023	-0.035 + 0.022	0.192 + 0.111	-0.343 + 0.180

The sensitivity to phase changes using a phase-conjugate mirror as the reference arm of the interferometer was demonstrated by the amount of defocus obtained from the data of Figures 10 and 11. The phase-conjugate interferometer allowed a much better effort at collimation than the method of measuring beam diameters. The amount of defocus using the beam diameter method is very small, yet is approximately 28 times greater than by a using the phase-conjugate interferometer to make further distance adjustments on the collimating lens. Acceptable values of aberrations are dependent upon the system requirements, but values in the range of an eighth to a quarter wave are common.

5.2   Plane Parallel Plates

Many parallel plates were tested in this experiment. Data for a glass plate, an aberrator consisting of a piece of cellophane tape on a microscope slide, and a thin film are shown in Figures 12-14. The Seidel coefficients
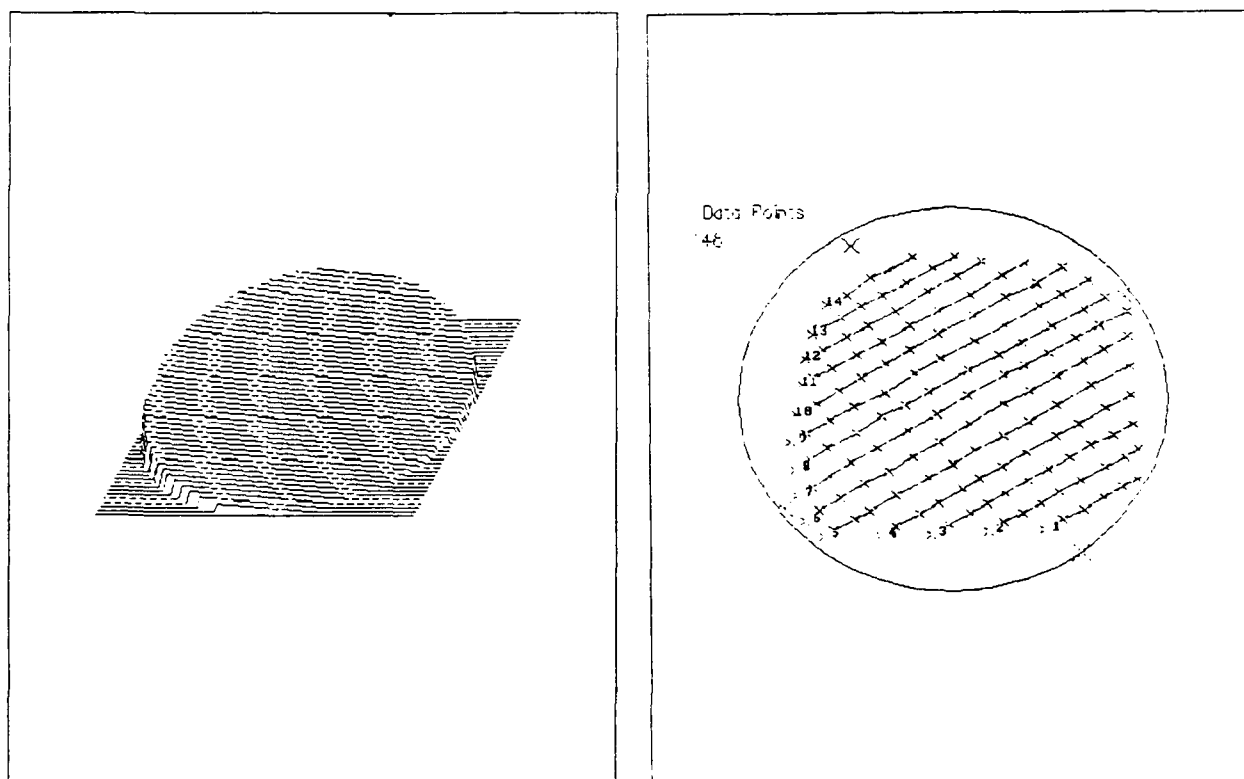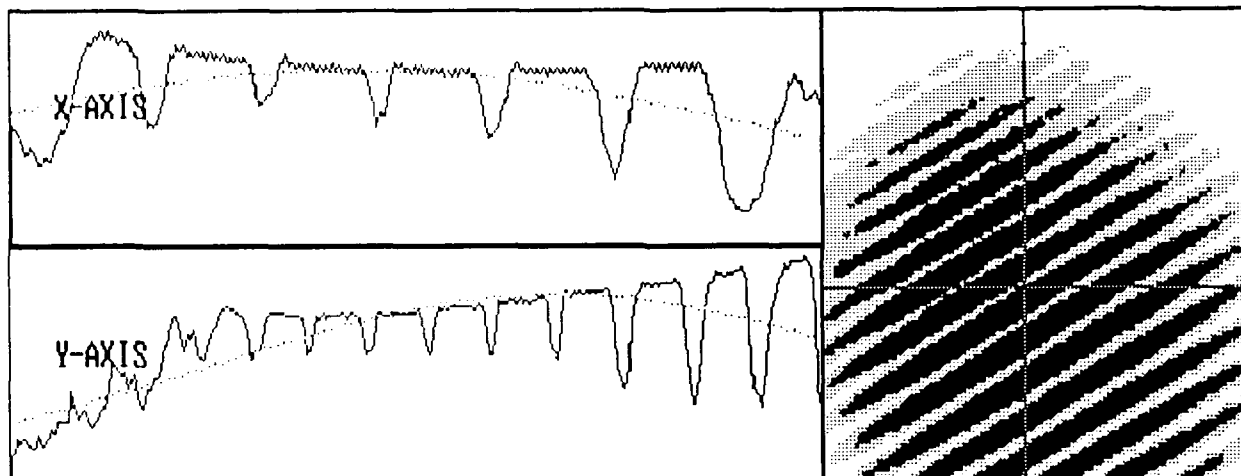
28

Figure 12.   Data for interferometry testing of a planar
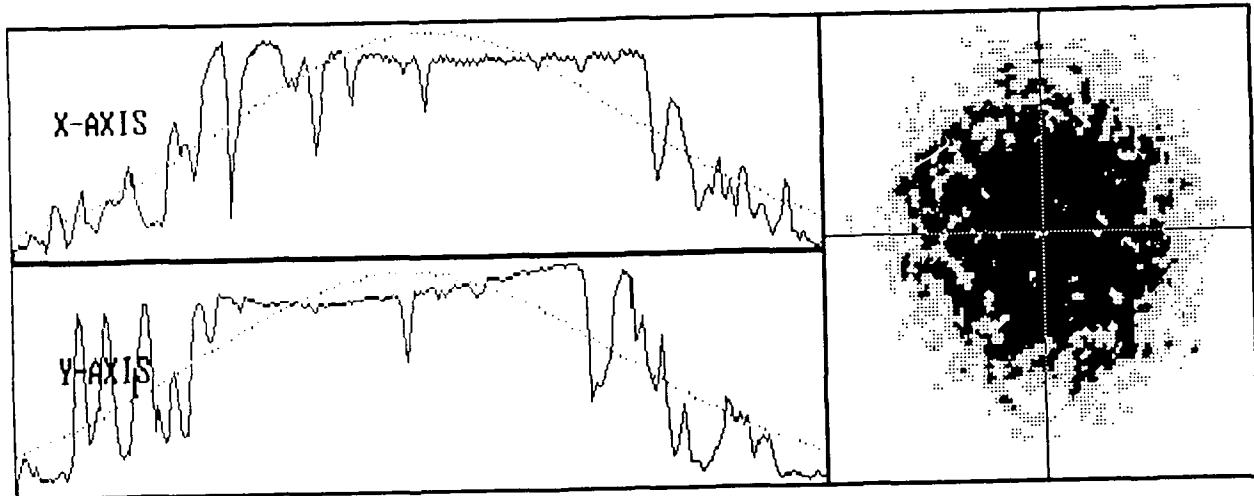glass plate

Figure 13. Data for interferometry testing of an aberrator

calculated from the digitization plots of Figures 12 and 14

are presented in Table 1.

The glass plate produced parallel straight fringes

(Figure 12) indicative of nonparallelism between the two

faces of the plate. There were 18 fringes across the

centimeter beam, giving a Δs of 5.55 x 10^5 nm. Using

Equation 4, and assuming a value of 1.5 for n, the tilt

between the plate faces is 9.26 x 10^-4 radians.

The microscope slide overlaid with cellophane tape

demonstrated (Figure 13) an interference pattern that

indicated the OPD varied greatly and no analysis could not

be performed on this data.

The thin film tested consisted of a soap bubble which

showed areas of increasing thickness (Figure 14) due to

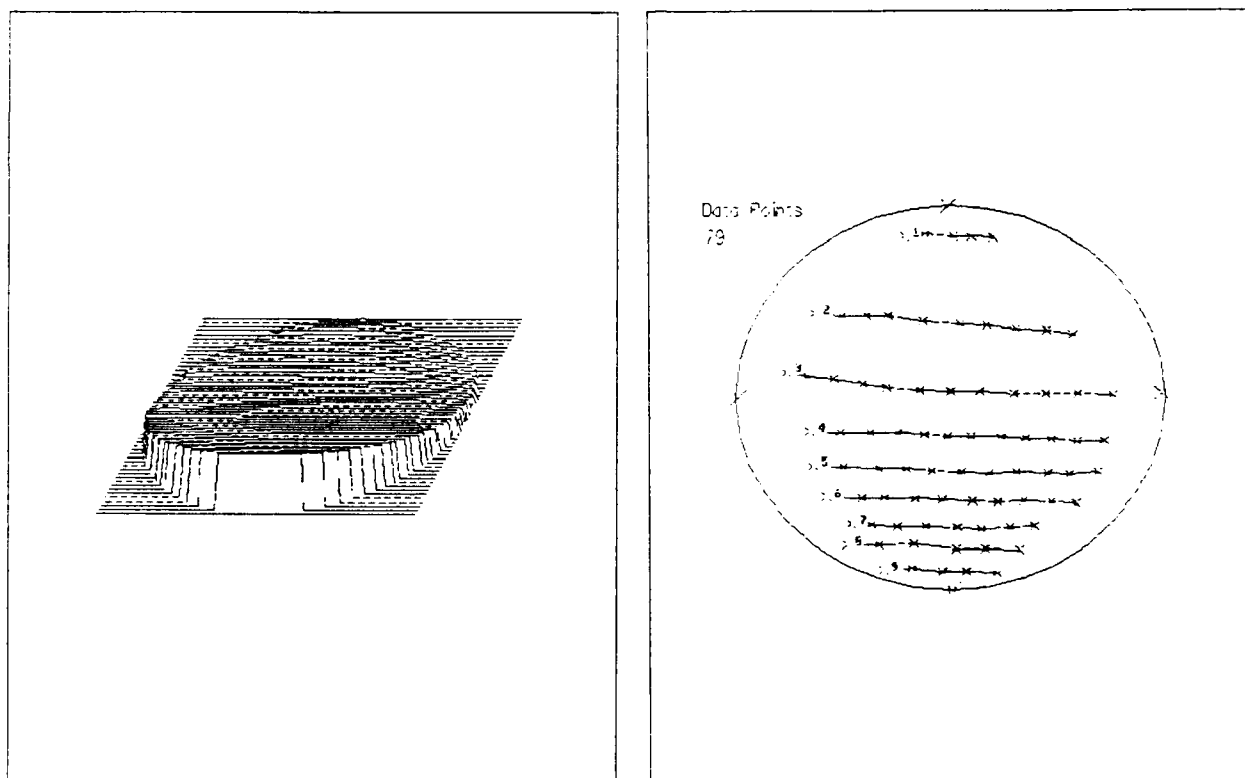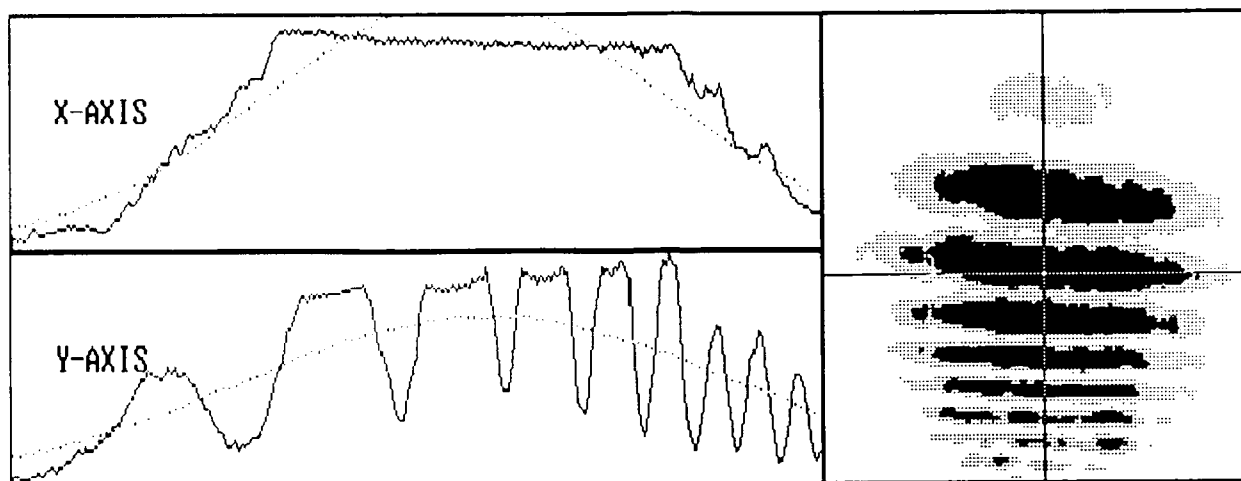gravitational pull on the material. This is evident by the

Figure 14. Data for interferometry testing of a thin film

31

decreasing width and distance of the fringes as the material increases in thickness.

The data for Figure 11 is a baseline for all collimated beam interferometry data; the difference between the values given for a particular test optic and those for Figure 11 is the actual value of the aberration introduced by the test optic. The glass plate and the thin film introduced amounts of astigmatism, coma, and spherical aberration which might be due to curvature of their surfaces.

5.3   Convergent Lenses

Figures 15-20 show the test data for three different convergent lenses. Data presented in Figures 15-18 was obtained for a good laboratory quality 170 mm plano-convex lens. Figures 19 and 20 present data collected for two different biconvex lenses, a 1.75 inch and a 150mm. The Seidel coefficients calculated from the digitization plots of Figures 15-18 are presented in Table 2 and Figures 19 and 20 presented in Table 3. The Seidel coefficients given by the WISP program show much higher standard deviations for spherical or astigmatic patterns. This introduces less confidence in the aberration data presented for these three lenses. Therefore, only trends for the amount of defocus and spherical aberration will be discussed.

The 170mm planar-convex lens of Figures 15-18 showed no aberration when it was correctly positioned at its focal length from the mirror as shown in Figure 8. Aberrations
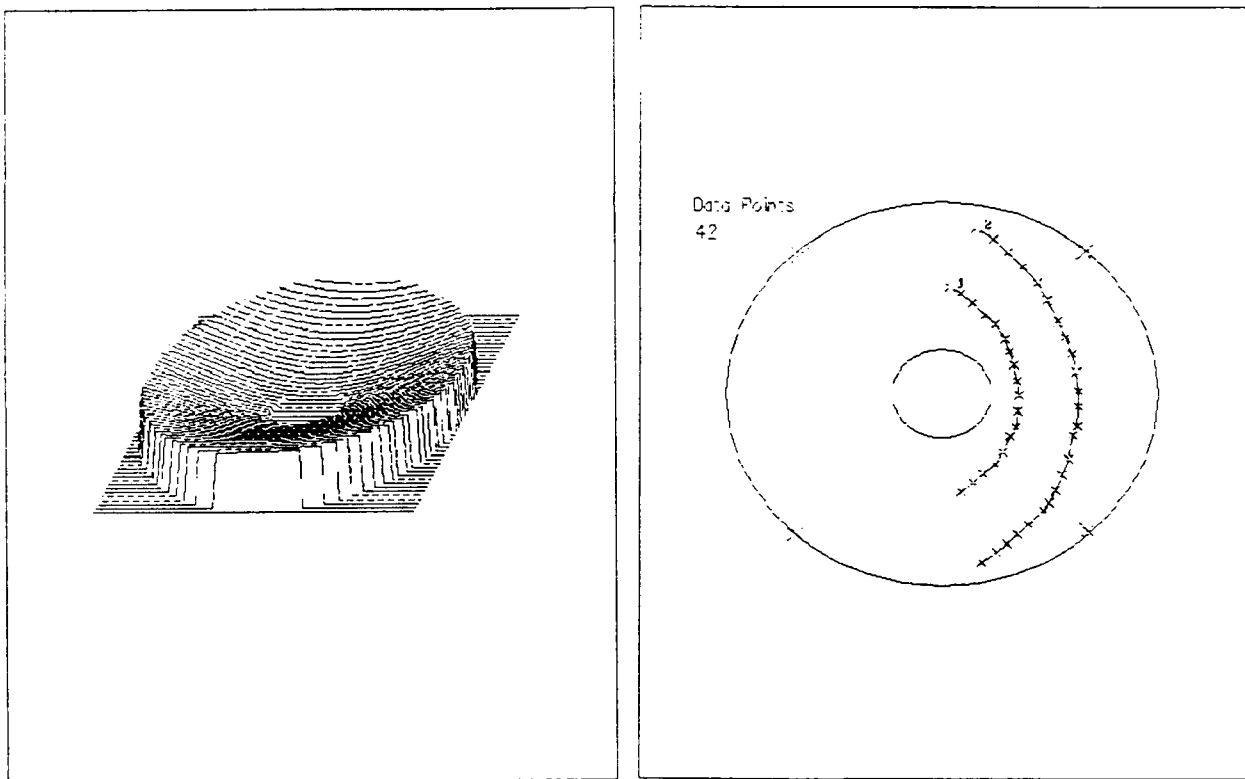
32

Figure 15. Data for interferometry testing of the 170mm
planar-convex lens when the mirror in the test arm was
located 0.25 cm behind the lens focal point and the planar
side of the lens faced the mirror

33

Figure 16. Data for interferometry testing of the 170mm
planar-convex lens when the mirror in the test arm was
located 0.25 cm in front of the lens focal point and the
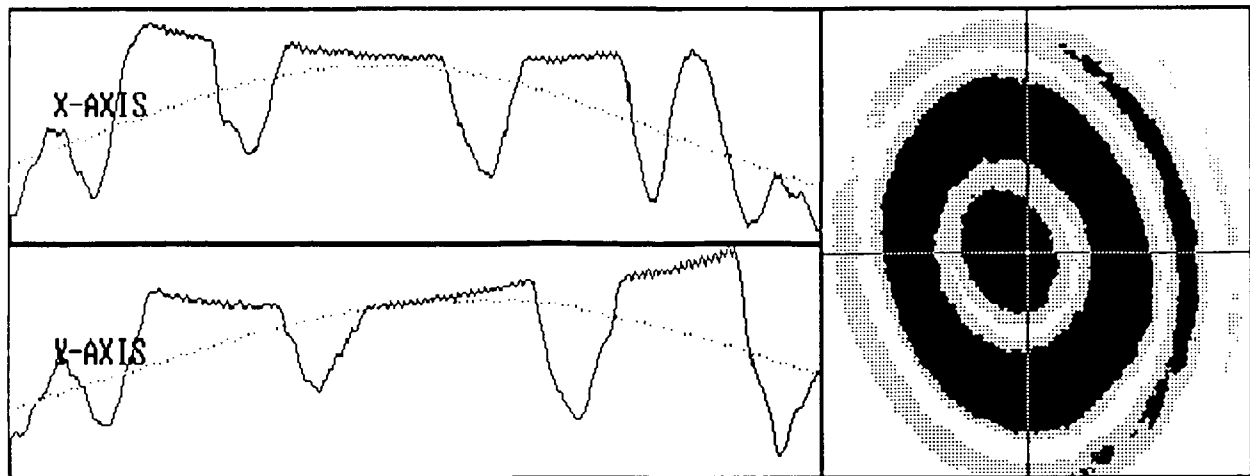planar side of the lens faced the mirror

Figure 17. Data for interferometry testing of the 170mm
planar-convex lens when the mirror in the test arm was
located 0.25 cm behind the lens focal point and the convex
side of the lens faced the mirror
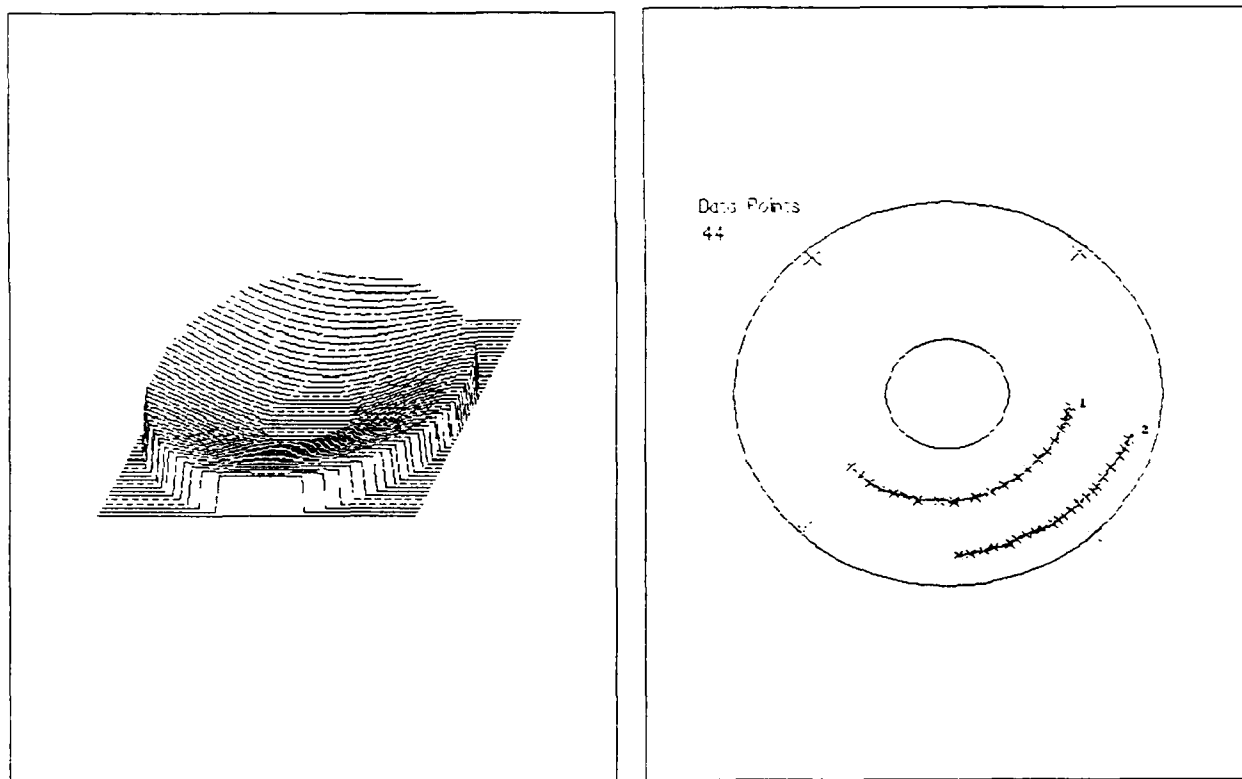
35

Figure 18. Data for interferometry testing of the 170mm
planar-convex lens when the lens was positioned at an angle
with respect to the plane mirror

36

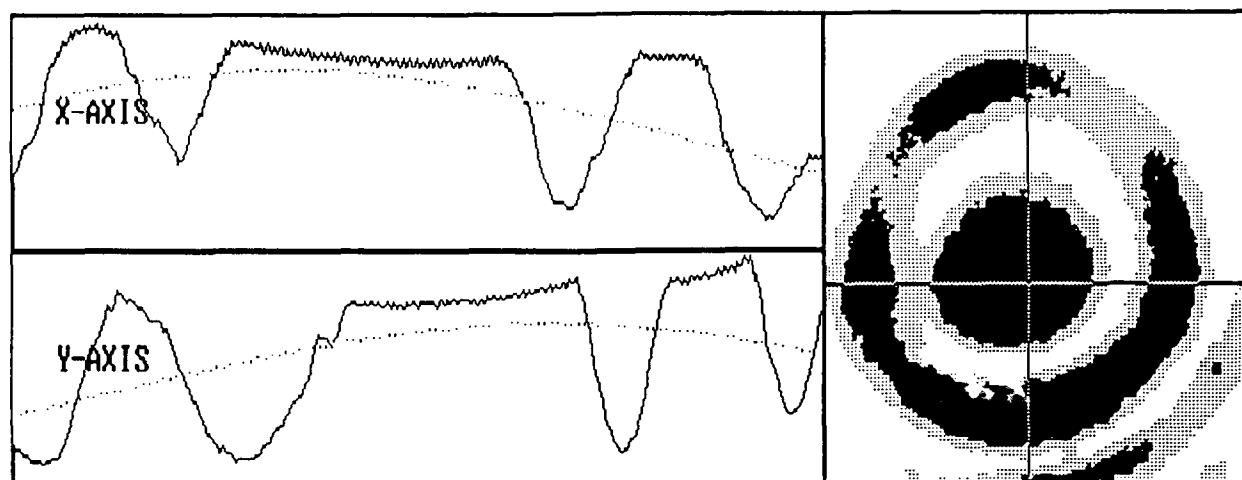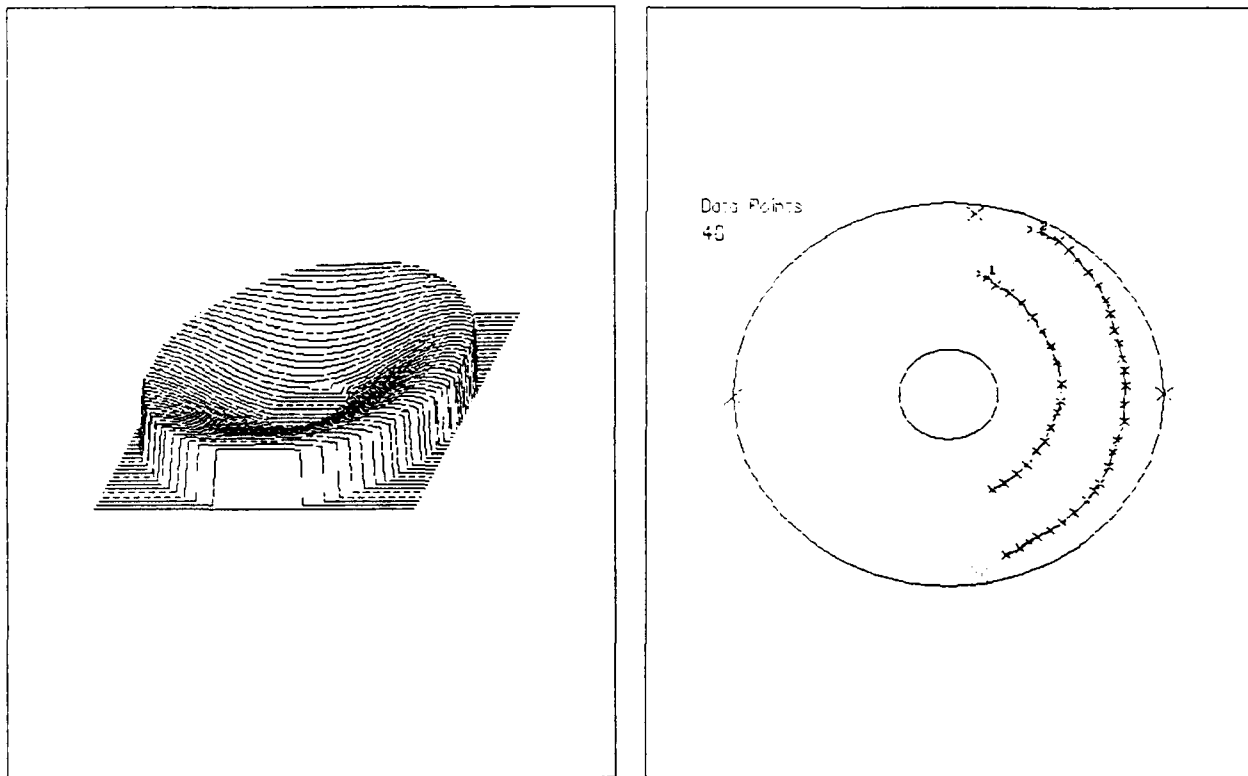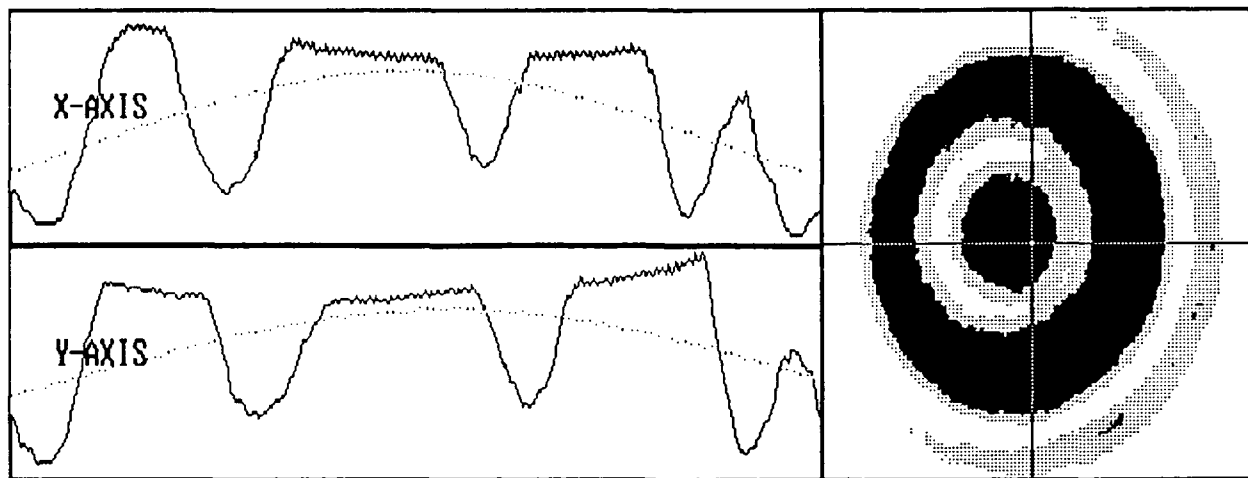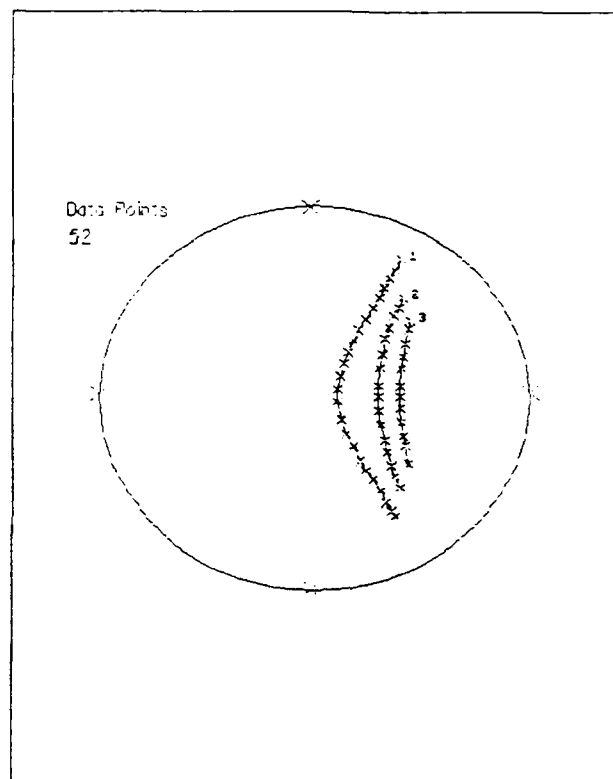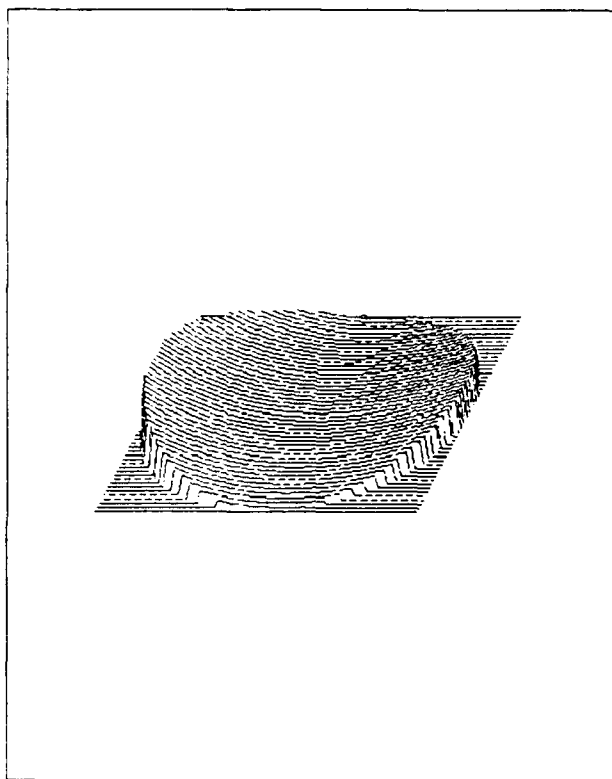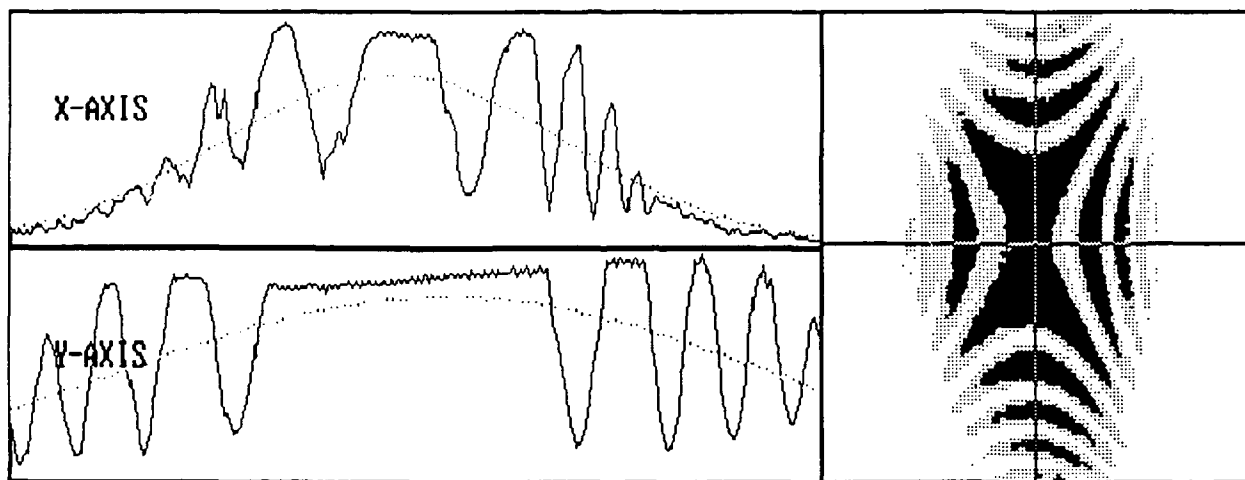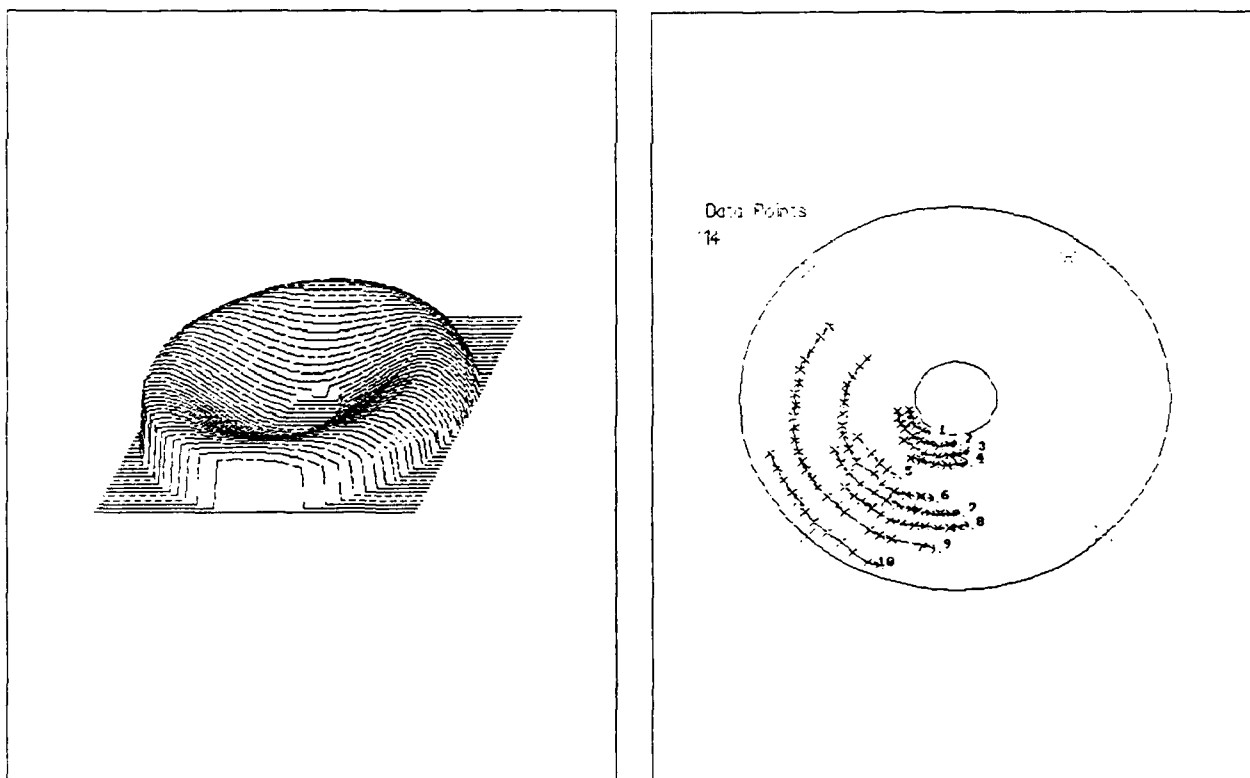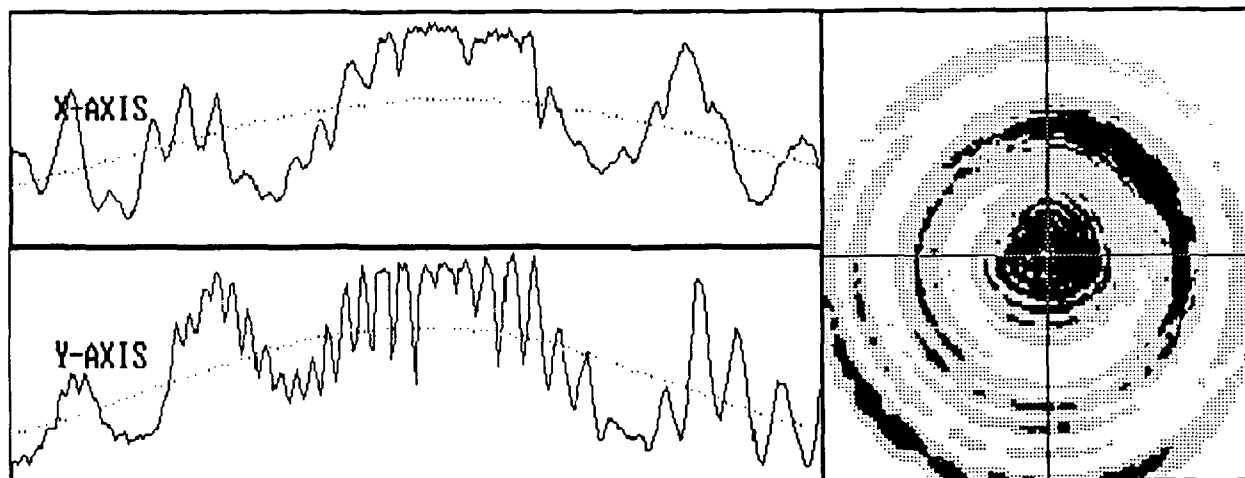Figure 19.   Data for interferometry testing of the 1.75 inch
biconvex lens
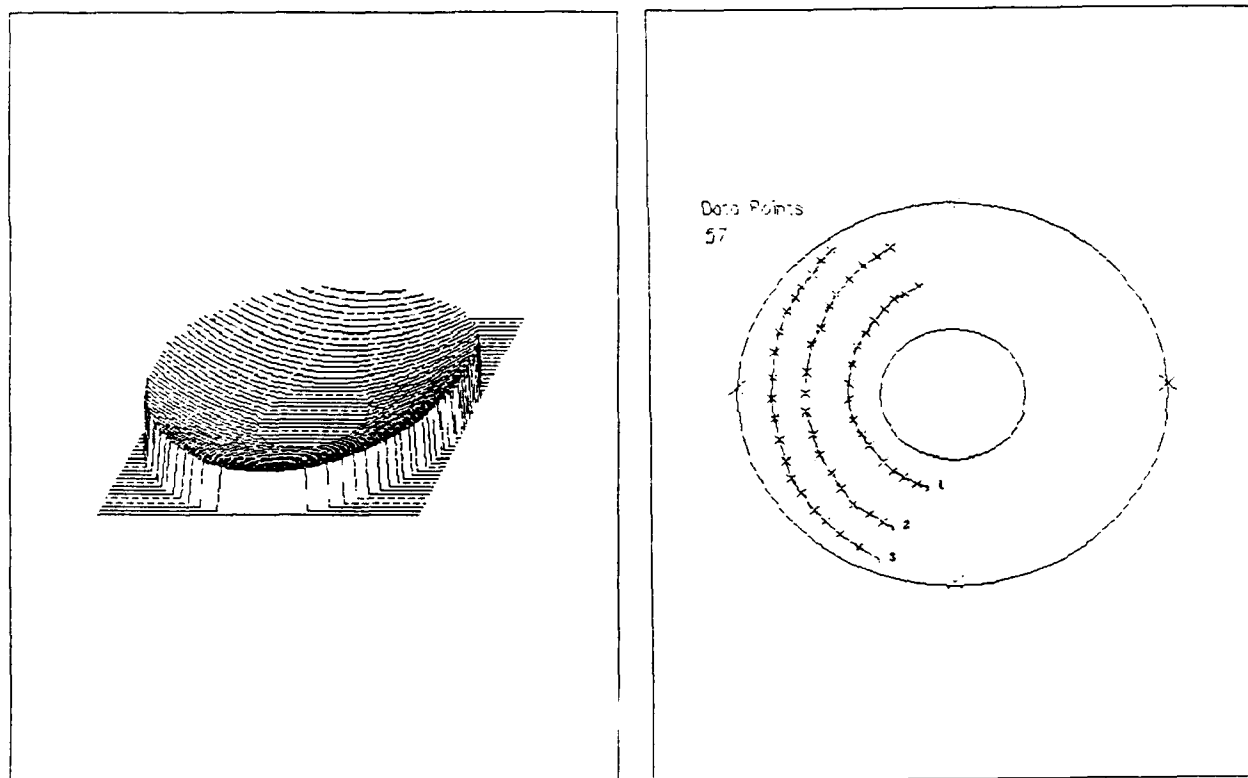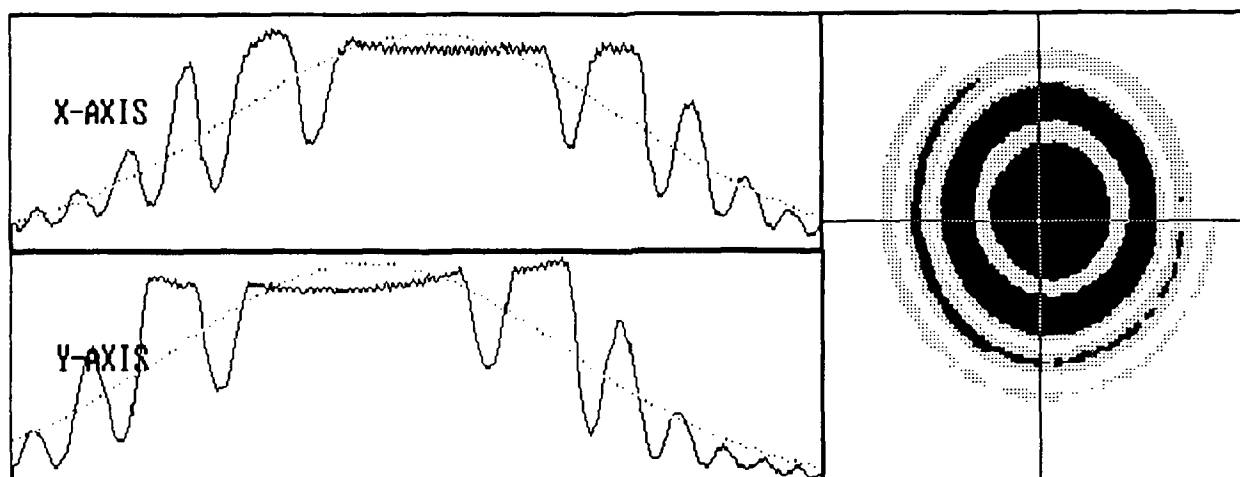
Figure 20. Data for interferometry testing of the 150mm
biconvex lens when the mirror in the test arm was located
0.25 cm behind lens focal point

TABLE 2

	FIGURE 15 Mirror behind *fp, planar side to mirror	FIGURE 16 Mirror forward of fp, planar side to mirror	FIGURE 17 Mirror behind fp, convex side to mirror	FIGURE 18 Lens at angle in input beam
TILT	1.407 ± 0.733	0.621 ± 0.226	1.327 ± 0.360	1.751 ± 0.784
DEFOCUS	3.283 ± 1.032	5.025 ± 1.259	5.394 ± 0.269	5.293 ± 1.380
ASTIGMATISM	0.388 ± 0.406	0.320 ± 0.140	0.193 ± 0.760	-15.588 ± 0.979
COMA	1.131 ± 0.862	1.019 ± 0.680	1.375 ± 0.467	1.196 ± 0.693
SPHERICAL ABERRATION	-1.210 ± 0.721	-2.246 ± 0.800	-2.806 ± 0.428	-0.832 ± 0.205

* fp = focal point

could be induced by moving the mirror away from the focal

point (fp) of the lens. For the data presented in

Figure 15, the planar side of the lens was facing the mirror

and the mirror was moved 0.25 cm behind the focal point of

the lens. Figure 16 is the same lens configuration but with

the mirror located 0.25 cm in front of the focal point of

the lens. Figure 17 is a repeat of the experiment that

produced the data for Figure 15, but the convex side of the

lens was facing the mirror. For the situations where the

mirror was located behind the lens focal point, the return

beam was as if from a further object point than that

required to return a collimated beam through the lens. When

the mirror was located forward of the lens focal point, the

opposite situation existed where the return beam was as if

from a closer object point. Both situations returned a

spherical wavefront, but focused to different points. At a
point prior to either beam reaching its focal point (the
observation screen), the return beam, when the mirror was
located behind the lens focal point (Figure 15), had a
longer radius of curvature since it had a focus point
further away. The amount of defocus and spherical
aberration was greater for the case with the smaller radius
of curvature (Figure 16). This is consistent with the
Seidel coefficients presented in Table 2 for these two
cases.

For the situation where the mirror was located behind
the lens focal point, testing was performed for two cases of
lens configuration; when the planar side (Figure 15) and
when the convex side (Figure 17) was facing the mirror.
More aberration was found in the case where the divergent
beams are incident upon the convex side of the lens due to
the greater difference between the angles the incident and
exit beams make with the lens surface normal. The amount of
defocus and spherical aberration in Figure 17 is greater
than that of Figure 15, as expected.

In Figure 18, the lens was positioned in the test arm
at an angle of 77 degrees with respect to plane mirror in
order to show astigmatism. The Seidel coefficients
presented in Table 2 indicate a large amount of astigmatism.

Several biconvex lenses were also tested. A poor
quality 1.75 inch biconvex lens was tested and showed
aberration when located at its focal length from the test

mirror (Figure 19). This lens showed a great deal of coma and spherical aberration. Since the interferogram pattern was highly irregular, there is less confidence in the digitization and amount of aberration determined for this lens.

Figure 20 is the data for a 150mm biconvex lens which showed no aberration when located at its focal length from the test mirror, but which produced the shown spherical pattern when the mirror in Figure 8 was located 0.25 cm beyond the focal length of the lens. This lens shows less aberration than the 170mm planar-convex lens tested in Figures 15-18. This is also a consequence of the small difference between the angles the incident and exit beam make with the normal.

5.4 Mirrors

Figure 21 shows the data obtained when using a commercial quality planar mirror in the basic experimental set-up. The quality of the fringes is deteriorated and a digitization is not presented. This mirror is not of high enough quality to use as the test mirror of the interferometer.

Data for the concave mirror which had a radius of curvature, R, of 0.5 meters is shown in Figures 22 and 23. The parallel infinite fringes found when the mirror was tilted and located a distance R from the pinhole of Figure 9
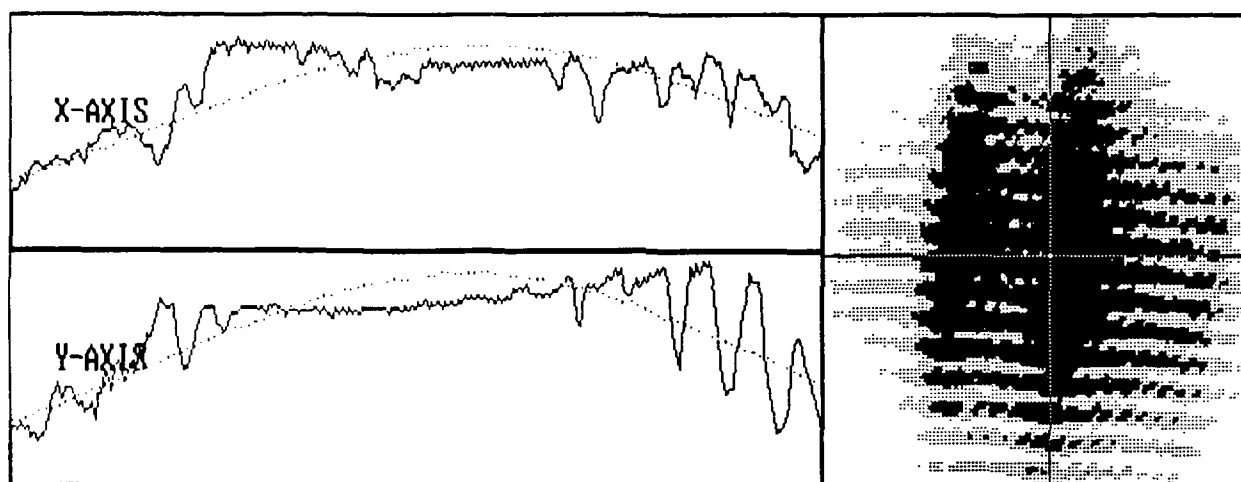
Figure 21. Data for interferometry testing of the
commercial quality plane mirror

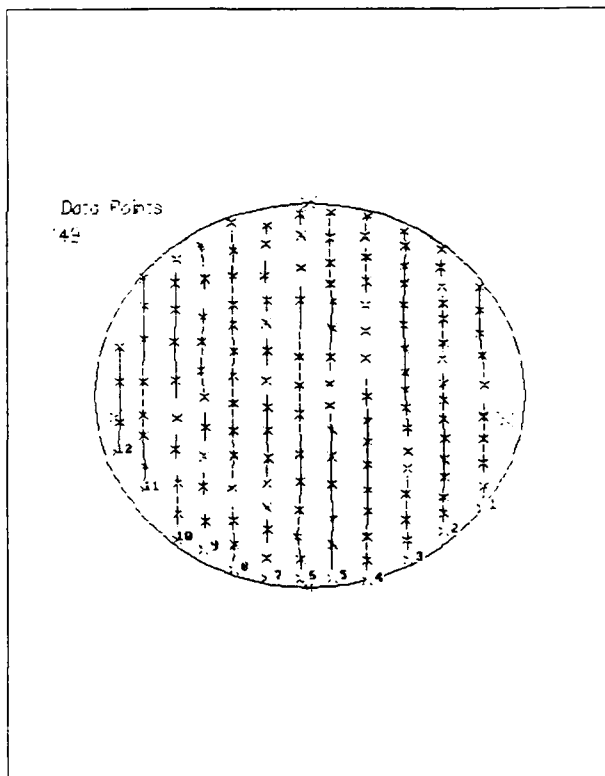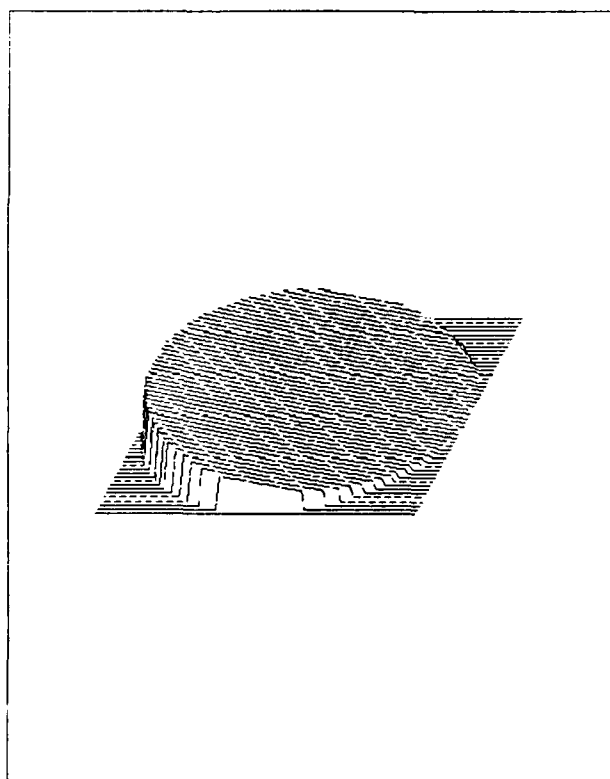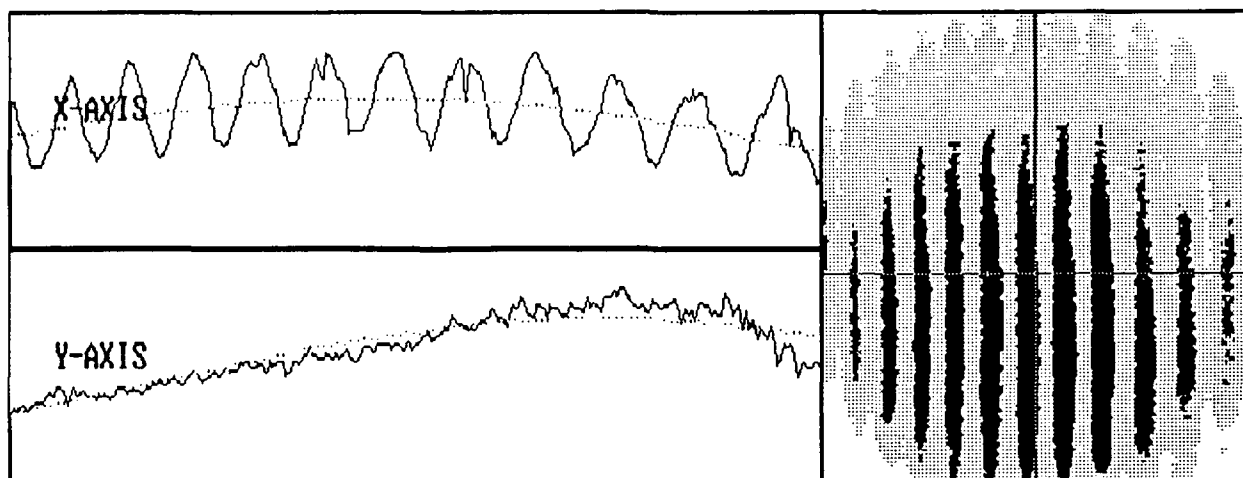Figure 22.   Data for divergent beam phase-conjugate
           interferometry testing of the concave mirror
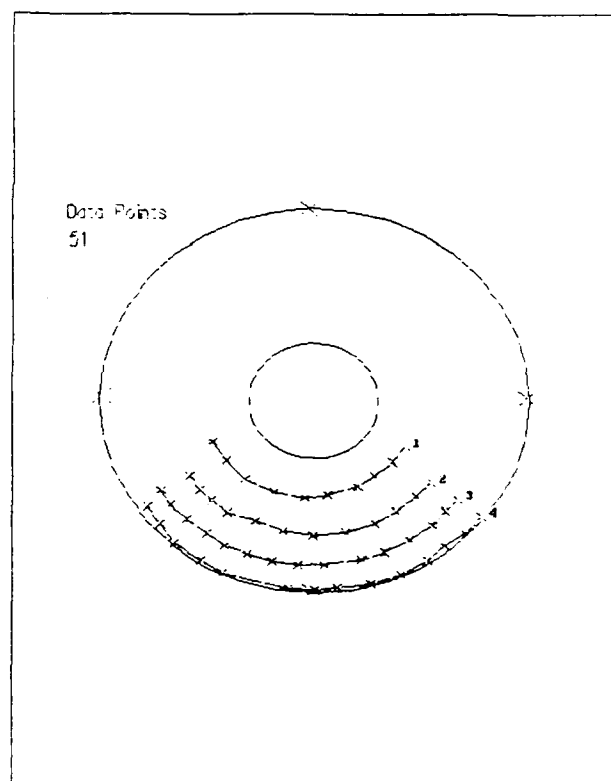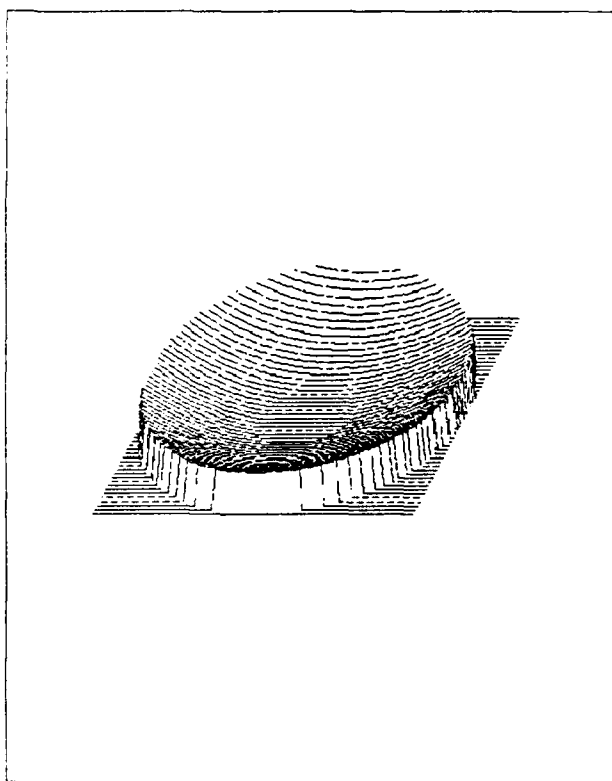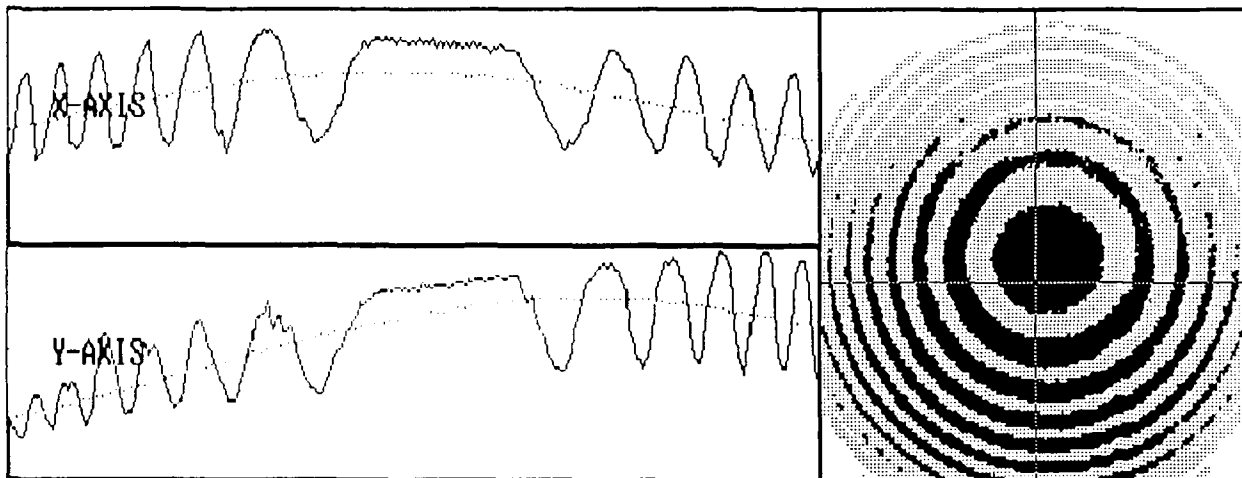
Figure 23. Data for divergent beam phase-conjugate
interferometry testing of the concave mirror when located
0.5 cm further from the pinhole

TABLE 3

SEIDEL COEFFICIENTS (IN WAVES) CALCULATED FROM THE DATA
PRESENTED IN FIGURES 19-20,22-23

	FIGURE 19 1.75" Biconvex lens	FIG 20 150mm Biconvex lens	FIG 22 Concave mirror at *fp	FIG 23 Concave mirror moved behind fp
TILT	4.493 ± 1.510	0.276 ± 0.038	6.382 ± 0.006	0.588 ± 0.355
DEFOCUS	23.943 ± 0.402	2.846 ± 0.175	0.850 ± 0.080	3.713 ± 0.555
ASTIGMATISM	1.739 ± 1.903	0.840 ± 0.141	0.720 ± 0.002	0.643 ± 0.261
COMA	7.416 ± 1.234	0.457 ± 0.250	0.051 ± 0.009	0.652 ± 0.221
SPHERICAL ABERRATION	-15.382 ± 5.289	-0.630 ± 0.54	-0.088 ± 0.076	0.193 ± 0.117

* fp = focal point

are recorded in Figure 22. A small amount of astigmatism was introduced due to this mirror, although no additional coma was evident and the uncertainty for spherical aberration makes a determination of this aberration present hard to define. Figure 23 shows the resultant interference pattern when the mirror is moved 0.5 cm further from the pinhole and the mirror tilt is almost eliminated. This interference pattern indicates that astigmatism, coma, and spherical aberration are present, but again, their uncertainties make a definite value of the aberration hard to define. Overall, this concave mirror is of good quality. It showed little aberration and the aberration found fall within acceptable ranges.

The Seidel coefficients calculated from the data in Figures 22-23 are presented in Table 3.

VI. Conclusions

In conventional Twyman-Green interferometry, any aberration present in the beam prior to being split into the two arms will cancel when the beams are recombined. When a phase-conjugate mirror is used in the reference arm, the interferometer will detect aberrations in the primary beam. Even a small amount of defocus in the primary beam is detectable when a phase-conjugate replica of the beam is interfered with its mirror image. This feature of phase-conjugate Twyman-Green interferometry makes it an extremely sensitive tool for determining beam collimation.

Another unique feature of phase-conjugate interferometry is that collimated or divergent beams may be used to test optics. Conventional Twyman-Green interferometry was also performed on the test optics in this thesis research. When testing the concave mirror using conventional methods (Figure 24), many advantages to the divergent phase-conjugate configuration were discovered.

In conventional Twyman-Green interferometry testing of the concave mirror, an additional optic needed to be placed in the test arm of the interferometer. This lens introduced additional reflections that needed to be considered and it needed to be extremely high quality in order that it did not introduce aberration to the interference pattern. Positioning the mirror in divergent beam so that it focused to a certain point was experimentally easier to
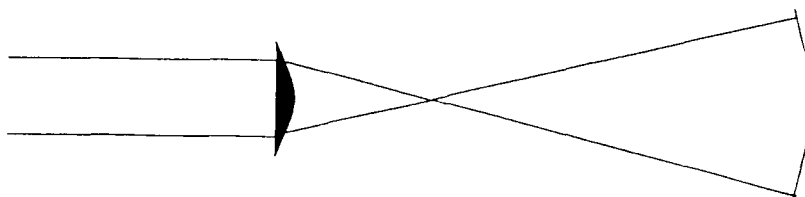
Figure 24.   Test arm configuration for conventional Twyman-
Green interferometry testing of a concave mirror

accomplish than to position the mirror with respect to the

lens in collimated beam testing such that the lens returned

collimated light.

The major sources of error in this experiment were the

digitization of fringes and the large standard deviation the

analysis package produced for circular or astigmatic

fringes. A better analysis package for determining

aberrations from actual intensity data files of the

interference pattern would greatly improve this experiment.

In conclusion, phase-conjugate Twyman-Green

interferometry was demonstrated and used for testing lenses,

plane plates, and mirrors. Divergent as well as collimated

beams could be used to test concave surfaces. This provides

47

a versatile tool for determining optical quality of concave
mirrors without the need of additional reference optics
normally required in conventional testing. The other major
feature of this type of interferometer was that it provided
a very sensitive test for collimated light. Unlike
conventional Twyman-Green interferometry, aberration in the
primary beam will be detected using the phase-conjugate
mirror in the reference arm.

Appendix A: Optic Components Used for Testing

Reference Number   LENSES

     1   150mm biconvex
     2   170mm plano-convex
     3   1.75" biconvex

                              MIRRORS

     4   lab quality planar
     5   lab quality concave (R = 0.5m)
     6   commercial quality
                           drug store planar

                       MISCELLANEOUS

     7   Glass plate
     8   Vu-graph transparency
     9   Thin film (Soap bubble)
    10   Microscope slide
                       w/cellophane tape

Appendix B: Zernike Polynomials and Determining Seidel Coefficients (WYCO 38,40)

Digitized fringe centers of an interferogram represent a loci of constant phase. These points are non-uniformly spaced across the vertical and horizontal axis of the pupil. By defining the extent of the pupil by the input fiduicals, the OPD value at each x,y location is normalized using the fringe order number and the total number of fringes. Zernike polynomials are used to interpolate this data to generate an array of OPD values on a uniform grid of 100 x 100 points. The data array is generated by fitting Zernike polynomials to the array of points using a Gram-Schmidt orthogonalization and the uniform grid array is filled using the Zernike polynomial fit.

Zernike polynomials are used since they consist of terms that are of the same form as the type of aberrations found in optical tests. Zernike polynomials are a complete set of polynomials in two real variables, ρ and θ, which are orthogonal over a unit circle. Zernike polynomials are distinguished from other sets of orthogonal polynomials by three properties. First, they have simple rotation symmetry properties that lead to a polynomial product of the form $R(\rho)G(\theta)$, where $G(\theta)$ is a continuous function which repeats itself every 2π radians and $G(\theta+\delta)=G(\theta)G(\delta)$. The trigonometric functions, $G(\theta)=e^{\pm im\theta}$, with m a positive integer or zero, satisfy this requirement, and are usually

represented as sines and cosines rather than complex
exponentials. The other two properties of Zernike
polynomials are that the radial function is a polynomial in
ρ of degree n and contains no power of ρ less than m, and
the radial function is even if m is even and odd if m is
odd.

The radial polynomials are a special case of Jacobi
polynomials and are listed as $R_n^m(\rho)$, with their
orthogonality and normalization given by

$$\int R_n^m(\rho) R_n^m(\rho) \, \rho \, d\rho = \frac{1}{2(n+1)} \delta_{nn} \tag{5}$$

and $R_n^m(1)=1$.

The radial polynomial can be factored

$$R_{2n-m}^m(\rho) = Q_n^m(\rho) \, \rho^m \tag{6}$$

where $Q_n^m(\rho)$ is a polynomial of order $2(n-m)$ and is
generally written as

$$Q_n^m(\rho) = \sum_{s=0}^{n-m} (-1)^s \frac{2(n-m-2)!}{s!(n-s)!(n-m-s)!} \rho^{2(n-m-s)} \tag{7}$$

The final Zernike polynomial series for the wavefront OPD,
ΔW, can be written

51

$$\Delta W = \overline{\Delta W} + \sum_{n=1}^{\infty} [A_n Q_n^0(\rho) + \sum_{m=1}^{n} Q_n^m(\rho) \rho^m (B_{nm} \cos(m\theta) + C_{nm} \sin(m\theta))] \quad \textbf{(8)}$$

where $\overline{\Delta W}$ is the mean wavefront OPD and A_n, B_{nm}, and C_{nm} are individual polynomial coefficients.

The Seidel coefficients indicating the amount of tilt, defocus, astigmatism, coma, and third order spherical aberration evident in a wavefront are computed from the first eight Zernike polynomials. These polynomials are listed below. Higher order aberrations can be computed from a higher number of terms in the polynomial expansion.

The Seidel coefficients were determined from the first eight Zernike polynomials:

1) $\rho \cos\theta$
2) $\rho \sin\theta$
3) $2\rho^2 - 1$
4) $\rho^2 \cos 2\theta$
5) $\rho^2 \sin 2\theta$
6) $(3\rho^2 - 2) \rho \cos\theta$
7) $(3\rho^2 - 2) \rho \sin\theta$
8) $6\rho^4 - 6\rho^2 + 1$

If the coefficients of the first eight Zernike polynomials are Z[1]...Z[8], then the Seidel coefficients are given by:

TILT
        x component $Z[1] - 2Z[6]$
        y component $Z[2] - 2Z[7]$
        magnitude = $(x^2 + y^2)^{1/2}$
        angle = $\tan^{-1}(y/x)$

DEFOCUS
        magnitude = $2Z[3] - 6Z[8] \pm (Z^2[4] + Z^2[5])^{1/2}$

        The sign is selected to minimize the absolute
        value of the magnitude.

52

ASTIGMATISM

magnitude $= \pm 2 (Z^2[4] + Z^2[5])^{1/2}$

angle $= \tan^{-1} (Z[5]/Z[4])$

The sign is opposite the sign used in the focus calculation.

COMA

magnitude $= 3 (Z^2[6] = Z^2[7])^{1/2}$

angle $= \tan^{-1}(Z[7]/Z[6])$

SPHERICAL ABERRATION

magnitude $= 6Z[8]$

For all angle measurements:
if numerator > 0 and denominator < 0, angle = angle - 180
if numerator < 0 and denominator < 0, angle = angle + 180

VII. Bibliography

Bar-Joseph, I. "Low-power phase-conjugate interferometry," Optics Letters, 6: 414-416 (September 1981).

Feinberg, Jack. "Interferometer with a self-pumped phase-conjugating mirror," Optics Letters, 8: 569-571 (November 1983).

Feinberg, Jack. "Continuous-Wave Self-Pumped Phase Conjugator with Wide Field of View," Optics Letters, 8: 480-482 (September 1983).

Gauthier, Daniel J. et al. "Phase-conjugate Fizeau interferometer," Optics Letters, 14: 323-325 (March 1989).

Hecht, Eugene and Alfred Zajac. Optics. Reading, Massachusetts: Addison-Wesley Publishing Company, 1979.

Hopf, Frederic A. "Interferometry using conjugate-wave generation," J. Opt. Soc. Am., 70: 1320-1323 (November 1980).

Howes, Walton L. "Lens collimation and testing using a Twyman-Green interferometer with a self-pumped phase-conjugating mirror," Applied Optics, 25: 473-474 (February 1986).

Malacara, Daniel. Optical Shop Testing. New York: Wiley & Sons, Inc., 1978.

Pepper, David M. et al. "The Photorefractive Effect," Scientific American, 62-74 (October 1990).

Schubert, Max and Bernd Wilhelmi. Nonlinear Optics and Quantum Electronics. New York: Wiley & Sons, Inc., 1986

Shukla, R. P. et al. "Phase conjugate Twyman-Green interferometer for testing spherical surfaces and lenses and for measuring refractive indices of liquids or solid transparent materials," Optics Communications, 78: 407-414 (September 1990).

Steel, W. H. Interferometry. Cambridge: Cambridge University Press, 1983.

Bibliography (cont.)

Wink, Lieutenant Karen A. _Laser Beam Coupling Via Optical Phase Conjugation in BaTiO₃._ MS Thesis, AFIT/GEP/ENP/88D-7. School of Engineering, Air Force Institute of Technology (AU), Wright-Patterson AFB, OH, December 1988 (AD-A202874).

Wyant, James C. _Optical Testing and Testing Instrumentation._ Optical Sciences Center, University of Arizona, 1987.

WYCO Interferogram Software Package, WISP-PC User's Guide version 2.3, WYCO Corp., Tuscon, AZ, 1986.

Vita

Captain Deborah A. Determan was born on 9 March 1958 in Olean, New York. She graduated from Archbishop Walsh High School in Olean in 1976. She graduated from Mississippi State University with a Bachelor of Science in Physics in May 1987, received a regular commission in the USAF and entered active duty on 15 Jan 1988 at Wright-Patterson AFB, Ohio. Her first assignment was as a Research Physicist at the Armstrong Medical Research Laboratory where she worked in the Modeling and Analysis Branch performing inertial property measurements, managed the laboratory program to develop test manikins for the Live Fire Test Program, was responsible for division involvement in Night Vision Goggle and Helmet Mounted Display development and testing, and performed computer simulations to investigate human and manikin head/neck response to g_z accelerations. She left the laboratory in May 1990 to enter the School of Engineering, Air Force Institute of Technology.

Permanent Address: 315 North 18th Street
                                        Olean, New York   14760

REPORT DOCUMENTATION PAGE

1. AGENCY USE ONLY (Leave blank)	2. REPORT DATE	3. REPORT TYPE AND DATES COVERED
	December 1991	Master's Thesis

4. TITLE AND SUBTITLE
Self-Pumped Phase-Conjugate Twyman-Green Interferometry
Using a BaTiO3 Crystal

5. FUNDING NUMBERS

6. AUTHOR(S)
Deborah A. Determan, Captain, USAF

7. PERFORMING ORGANIZATION NAME(S) AND ADDRESS(ES)

Air Force Institute of Technology
WPAFB OH 45433-6583

8. PERFORMING ORGANIZATION REPORT NUMBER

AFIT/GEP/ENP/91D-3

9. SPONSORING / MONITORING AGENCY NAME(S) AND ADDRESS(ES)

PL/LTN

Kirtland AFB NM 87117-6008

10. SPONSORING / MONITORING AGENCY REPORT NUMBER

11. SUPPLEMENTARY NOTES

12a. DISTRIBUTION / AVAILABILITY STATEMENT

Approved for public release; distribution unlimited

12b. DISTRIBUTION CODE

13. ABSTRACT (Maximum 200 words)
This study demonstrated a phase-conjugate Twyman-Green interferometer using a
BaTiO3 crystal in the reference arm and this interferometer was used to test
various optical components. This was done using both collimated and divergent
beams as the primary beam. Testing was performed to determine optical quality of
various convergent lenses, plane parallel plates, and planar and concave mirrors.
Phase-conjugate interferometry using a divergent beam provided a technique to test
concave mirrors without the need of additional high quality optics normally needed
for this type of testing using conventional Twyman-Green interferometers.
Additionally, a phase-conjugate interferometer is able to detect with twice the
sensitivity any defect in the primary beam This property makes the phase-
conjugate interferometer a highly sensitive test for collimation.

14. SUBJECT TERMS
Phase Conjugation, Nonlinear Optics, Interferometry
Barium Titanate, Optical Testing

15. NUMBER OF PAGES
64

16. PRICE CODE

17. SECURITY CLASSIFICATION OF REPORT	18. SECURITY CLASSIFICATION OF THIS PAGE	19. SECURITY CLASSIFICATION OF ABSTRACT	20. LIMITATION OF ABSTRACT
Unclassified	Unclassified	Unclassified	UL